SANDIA REPORT
SAND2001-2674
Unlimited Release
Printed August 2001

Structural Foam Characteristics in a Mechanical Shock Environment

Vesta I. Bateman, Fred A. Brown, and Darren A. Hoke

Prepared by
Sandia National Laboratories
Albuquerque, New Mexico 87185 and Livermore, California 94550

Sandia is a multiprogram laboratory operated by Sandia Corporation, a Lockheed Martin Company, for the United States Department of Energy under Contract DE-AC04-94AL85000.

Sandia National Laboratories

Issued by Sandia National Laboratories, operated for the United States Department of Energy by Sandia Corporation.

Available to DOE and DOE contractors from
U.S. Department of Energy
Office of Scientific and Technical Information
P.O. Box 62
Oak Ridge, TN 37831

Telephone: (865)576-8401
Facsimile: (865)576-5728
E-Mail: reports@adonis.osti.gov
Online ordering: http://www.doe.gov/bridge

Available to the public from
U.S. Department of Commerce
National Technical Information Service
5285 Port Royal Rd
Springfield, VA 22161

Telephone: (800)553-6847
Facsimile: (703)605-6900
E-Mail: orders@ntis.fedworld.gov
Online order: http://www.ntis.gov/ordering.htm

SAND 2001-2674
Unlimited Release
Printed August 2001

Structural Foam Characteristics in a Mechanical Shock Environment

Vesta I. Bateman, Fred A. Brown, and Darren A. Hoke
Engineering Sciences Center
Sandia National Laboratories
P. O. Box 5800
Albuquerque, NM 87185-0553

Abstract

At Sandia National Laboratories (SNL), structural foam is used to mitigate the shock created in structures during impact and to isolate the internal components from this shock. Split Hopkinson Bar experiments were conducted to investigate the high-rate strain rate characteristics of 10 pcf and 20 pcf rigid closed-cell polyurethane foam. Right circular cylinders of diameter 0.75 in. and lengths of 0.75 in. and 1.50 in. were subjected to impulsive compressive loading at average strain rates of 640 $sec.^{-1}$. Samples (0.75 in. diameter) were subjected to compressive impulsive loading at average strain rates of 1370, 2740, 3200, and 6400 $sec.^{-1}$. To investigate the effect of confining pressure, samples were tested in radially confined (and unconfined) configurations. Radially confined samples were prepared by pouring the uncured foam mixture into 0.125 in.-thick-walled steel cylinders to cure for lengths of 0.15, 0.35, 0.75 in., and 1.50 in. Experimental results are presented as stress-strain plots. High-speed photometric measurements of the 0.15 and 0.35 in. lengths during Hopkinson bar test show $\approx$ 5% change in area, so the stress-strain plots may be considered true stress-true strain plots for these two lengths. Post-test optical microstructure analysis concludes that the level of damage in the PMDI foams increased with increases in average strain rate and decreases in sample thickness.

Contents

Figures

Figures (cont.)

Tables

Structural Foam Characteristics in a Mechanical Shock Environment

Introduction

The purpose of the structural foam in the B61 bomb is to mitigate the mechanical shock created upon impact and to isolate the internal components from this shock. The mitigation is accomplished by three mechanisms. First, the foam has much lower impedance than the aluminum case, and this impedance mismatch prevents some of the shock from entering the foam. Second, the foam absorbs energy and thereby reduces the magnitude of the shock. Finally, the foam is loaded and unloaded by the shock as it passes through the material. This loading and unloading of the foam even in the elastic regime will dissipate energy due to the hysteresis that these materials exhibit

The foam in the B61 Short Stack (Inner Case Assembly) has been changed from Toluene Di-Isocyanate* (TDI) to Polymethylene Polyphenyl Isocyanate* (PMDI). PMDI is also known as Polymethylene Polyphenol Isocyanate* (PAPI) which is Dow-Corning's* trade name for PMDI. Tests have been performed to characterize the shock mitigating properties of the PMDI foam. Results from the Split Hopkinson Bar [1,2] experiments of the PMDI foam are presented in this report and provide characterization of the shock mitigating properties of the foam by impedance mismatch in both constrained and unconstrained geometries. The foam samples were provided by Don Watson of Honeywell (formerly Allied Signal Aerospace); the specifications for the foam samples are shown in Table I. Although the structural foam in the B61 is generally considered constrained, both unconstrained and constrained tests have been conducted to determine the effect(s) of the confinement. The radially unconfined samples were prepared by machining individual samples from a large block of foam. The radially confined samples were prepared by pouring the uncured foam mixture into individual steel tubes to maintain microstructural uniformity as a function of length. The samples cured with plates to confine the ends. The plates did not have vent holes and did have mold release to maintain uniform end surfaces. These data provide new dynamic characteristics that can be used to improve foam models that currently have static characteristics only [3].

---

*Reference to a commercial product implies no endorsement by SNL or the Department of Energy or lack of suitable substitute.

Table I: Specifications for Foam Samples.

Quantity	10 pcf Density	20 pcf Density
Foam System	BKC 44307-4	BKC44306-10
T Component	2170421	2170678
R Component	2170425	2170422

Hopkinson Bar Experimental Configuration

This study was conducted with a split Hopkinson bar experimental configuration shown in Figure 1. The two Hopkinson bars are made of 6061T6 aluminum and have a length of 48 in. Each foam sample was placed between the two aluminum bars. The bars and material samples have a nominal 0.75 in. diameter. The incident bar is the bar impacted by the air gun projectile. The transmission bar is the bar beyond the sample. Strain gages were mounted in the middle of the bar at 24 in. for both the incident bar and the transmission bar. Strain gages were mounted on the bars with AE-10 epoxy. This epoxy was used because anomalies were observed in the data obtained with strain gages mounted with lower strength (and quicker curing) epoxies. The nominal applied load as the incident compressive wave measured as particle velocity have a 40 fps peak with a 100 μs duration (measured at 10% amplitude) and 80 fps peak with a 100 μs duration (measured at 10% amplitude) for these experiments. Incident, reflected, and transmitted strains were measured for each experiment using the strain gages, and these measurements provided the basis for characterizing the foam material.

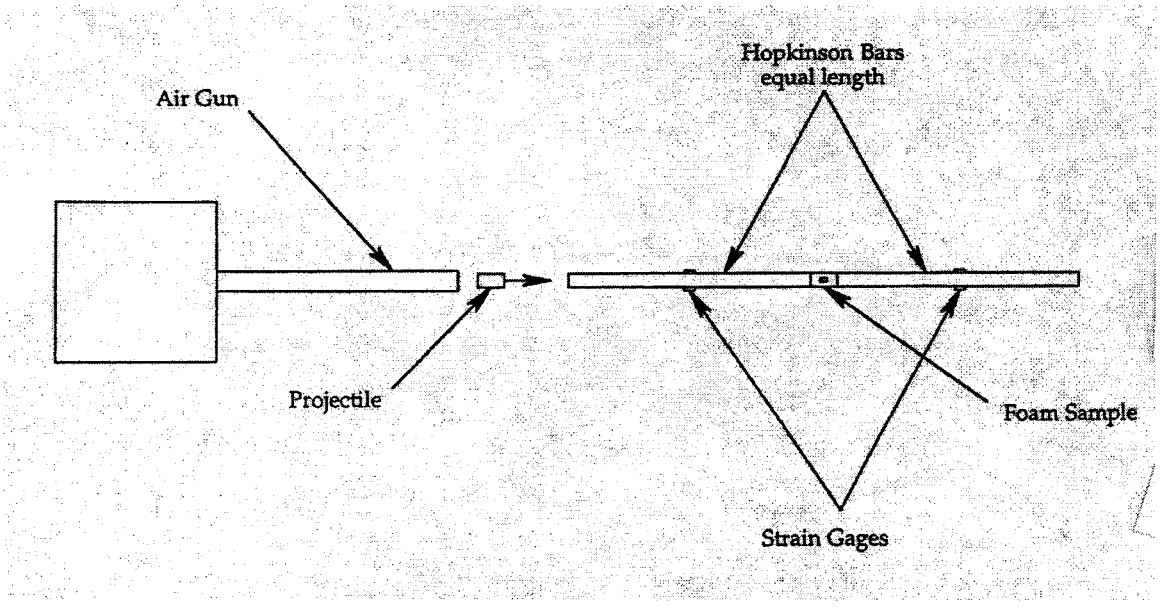

Figure 1. Split Hopkinson Bar Configuration for PMDI Foam Characterization.

Considerable effort was made during the initial portion of the experiments to align the two aluminum bars. The bars are positioned using two-axis alignment stages made by Newport. Each Hopkinson bar has a two-axis alignment stage on each end. The bars are aligned to minimize the reflection at the bar-to-bar interface without any foam material in between the bars. Figure 2 shows the incident and reflected wave achieved with the best alignment obtainable for this experimental configuration. Dow Corning 321 Dry Film Lubricant gave the least reflection at the interface. The reflected wave occurs at about 225 μs and has a magnitude of -100 psi or 0.81% of the incident stress wave. This alignment was judged by the authors as acceptable for these split Hopkinson bar experiments.

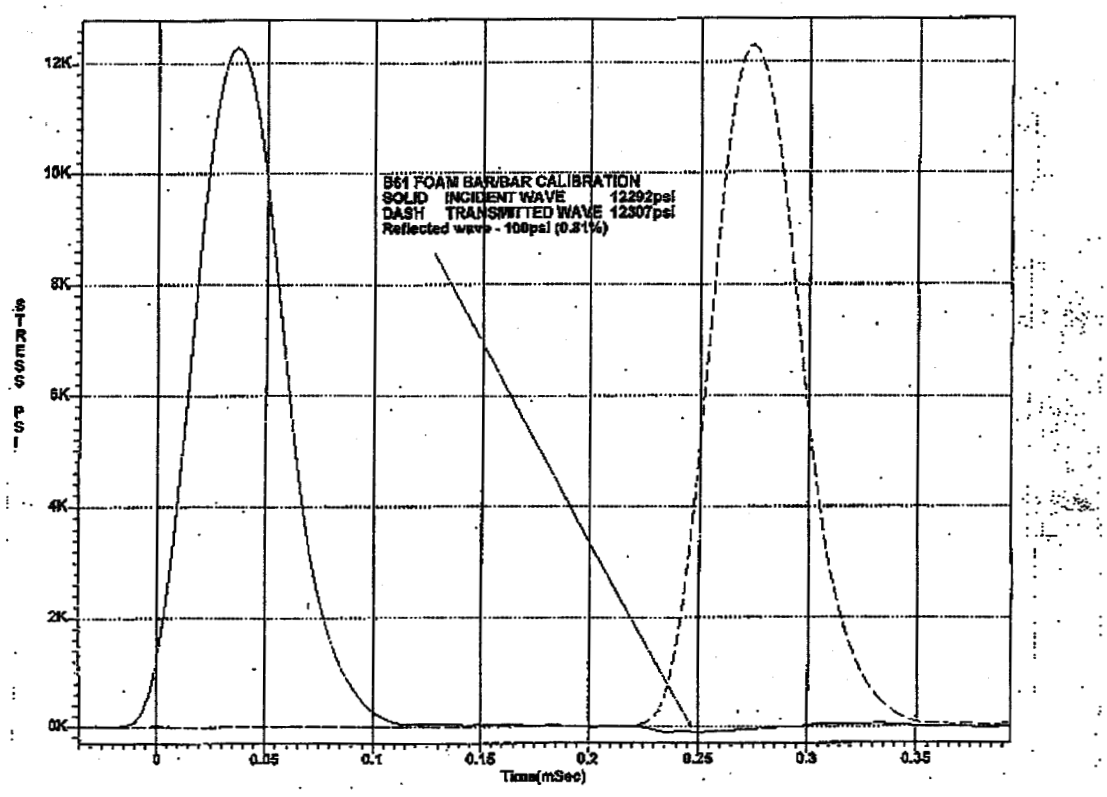

Figure 2: Incident and Reflected Stress Waves for Initial Bar to Bar Alignment.

Hopkinson Bar Data Analysis and Results

An initial matrix of materials and geometries are shown in Table II. These tests were conducted at one strain rate, $\dot{\varepsilon}$, 640 sec.$^{-1}$, where strain rate is defined as [1]:

$$\dot{\varepsilon} = \frac{V}{L} \tag{1}$$

and V is the peak particle velocity of the stress wave in the Hopkinson bar and L

Table II: Test Parameters for Initial Testing of 10 pcf and 20 pcf in Constrained and Unconstrained Geometries.

Length	Velocity
0.75 in.	40 fps
1.50 in.	80 fps

is the length of the foam sample. Only one sample for each condition in Table II was tested. The strain gages are calibrated in particle velocity to obtain the peak, V, measurement. Equation (1) depends on the sample undergoing ***homogeneous*** deformation. Therefore, the strain rates in this report should be considered ***average strain rates*** in some cases. The parameters in Table II were used to determine the foam performance at two different velocities and two different sample lengths that have the same strain rate, 640 sec.$^{-1}$.

The data from all the split Hopkinson bar tests was analyzed to obtain force and displacement according to the equations below [1].

$$\delta_s(t) = -2\int C_o \varepsilon_r(t)dt = \text{Sample Displacement} \qquad (2)$$

$$F_s(t) = A_b E_{bar} \varepsilon_t(t) = \text{Force Applied to Sample} \qquad (3)$$

where $\delta_s(t)$ is the sample displacement as a function of time, C_o is the longitudinal bar velocity, $\varepsilon_r(t)$ is the reflected strain, $F_s(t)$ is the force applied to the sample, A_b is the cross-sectional area of the bar, E_{bar} is Young's modulus of the bar material, and $\varepsilon_t(t)$ is the transmitted strain. A cross-plot of stress as a function of strain is made to obtain the final result.

The stress-strain-plots for the initial test matrix are shown in Figures 3-6 . Figures 3 and 4 are for unconstrained foam with the densities of 10 pcf and 20 pcf, respectively. Figures 5 and 6 are for the constrained foam with the densities of 10 pcf and 20 pcf, respectively. For these plots, the force was divided by the cross-sectional area of the sample to obtain stress (psi), and the sample displacement was divided by the sample length to obtain strain (in/in). This conversion of force and displacement into stress and strain assumes that the sample dimensions do not change significantly during the measurements.

The results in Figures 3-6 indicate that the PMDI foam has approximately the same maximum stress for the strain rate of 640 sec.$^{-1}$and the two velocities of 40 and 80 fps. For the unconstrained samples, the results for the two densities show that there is a sharp increase in stress for small strains and then a constant level of stress for larger strains. For the constrained samples, there is a more linear increase in the stress as a function of strain. The 20 pcf foam is four times

stronger than the 10 pcf foam at these lengths and velocities. Additionally, the constrained samples for both densities show an increased strength of 67%. Table III summarizes the peak stress levels for the tests at a strain rate of 640 sec.$^{-1}$.

Table III: Summary of Peak Stress Values for Split Hopkinson Bar Tests at 640 sec^{-1} Strain Rate.

Geometry	10 pcf Density	20 pcf Density
Unconstrained	300 psi	1200 psi
Constrained	500 psi	2000 psi

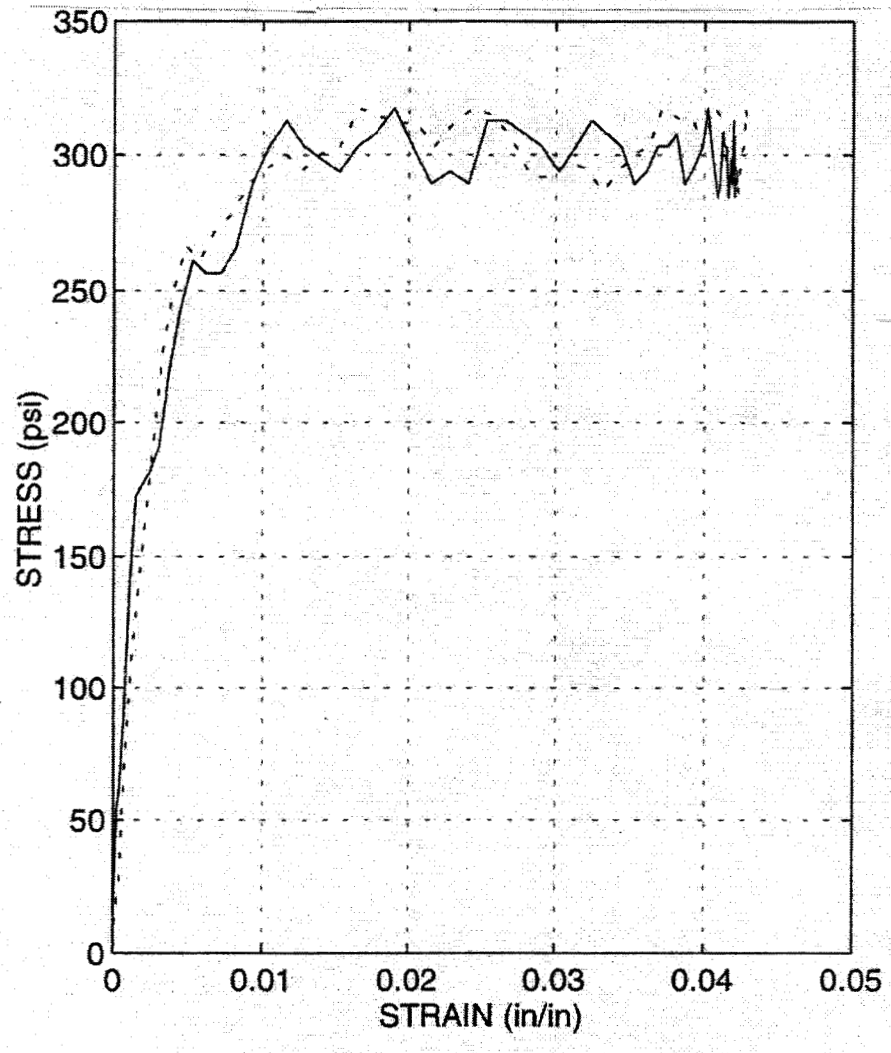

Figure 3: Unconstrained PMDI Foam with 10 pcf Density and 640 sec^{-1} Strain Rate
Solid – 40 fps Peak Velocity and 0.75 in. Length
Dashed – 80 fps Peak Velocity and 1.50 in. Length

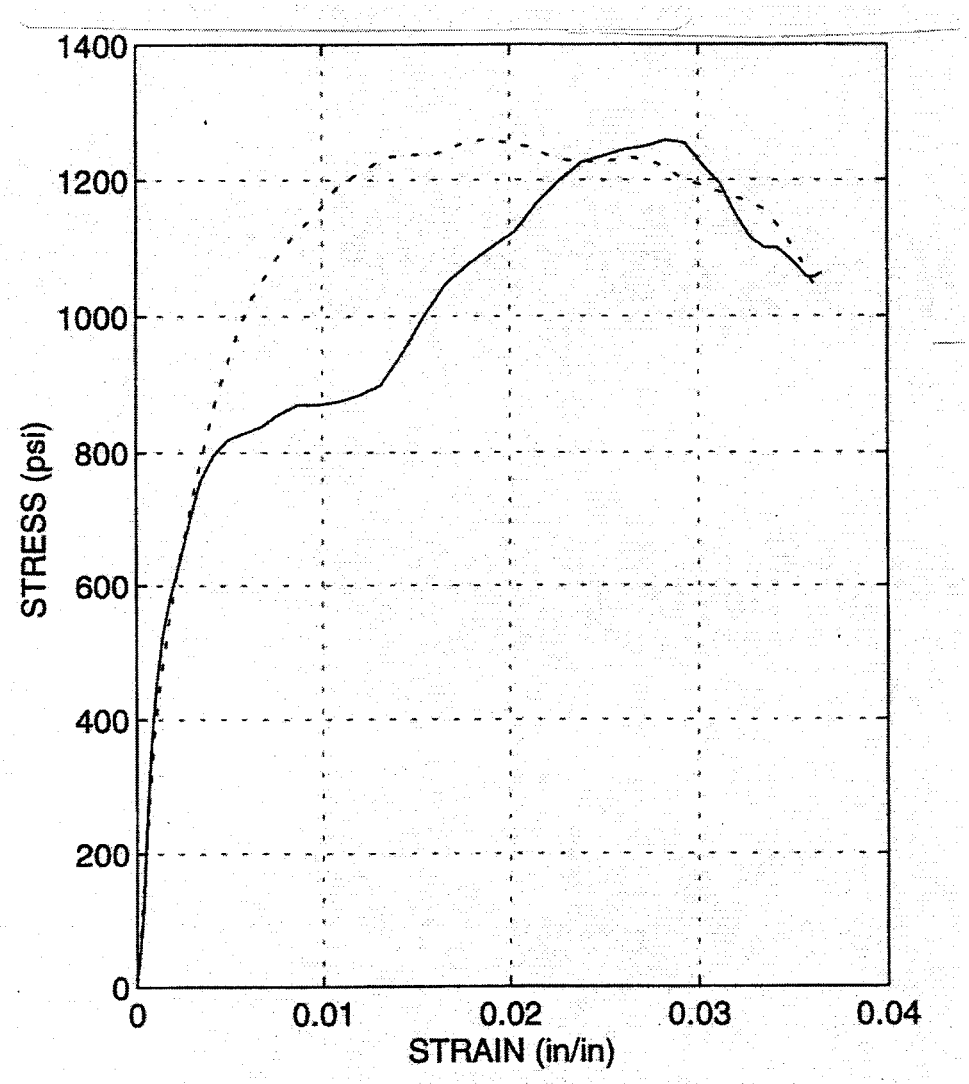

Figure 4: Unconstrained PMDI Foam with 20 pcf Density and 640 sec^{-1} Strain Rate
Solid – 40 fps Peak Velocity and 0.75 in. Length
Dashed – 80 fps Peak Velocity and 1.50 in. Length

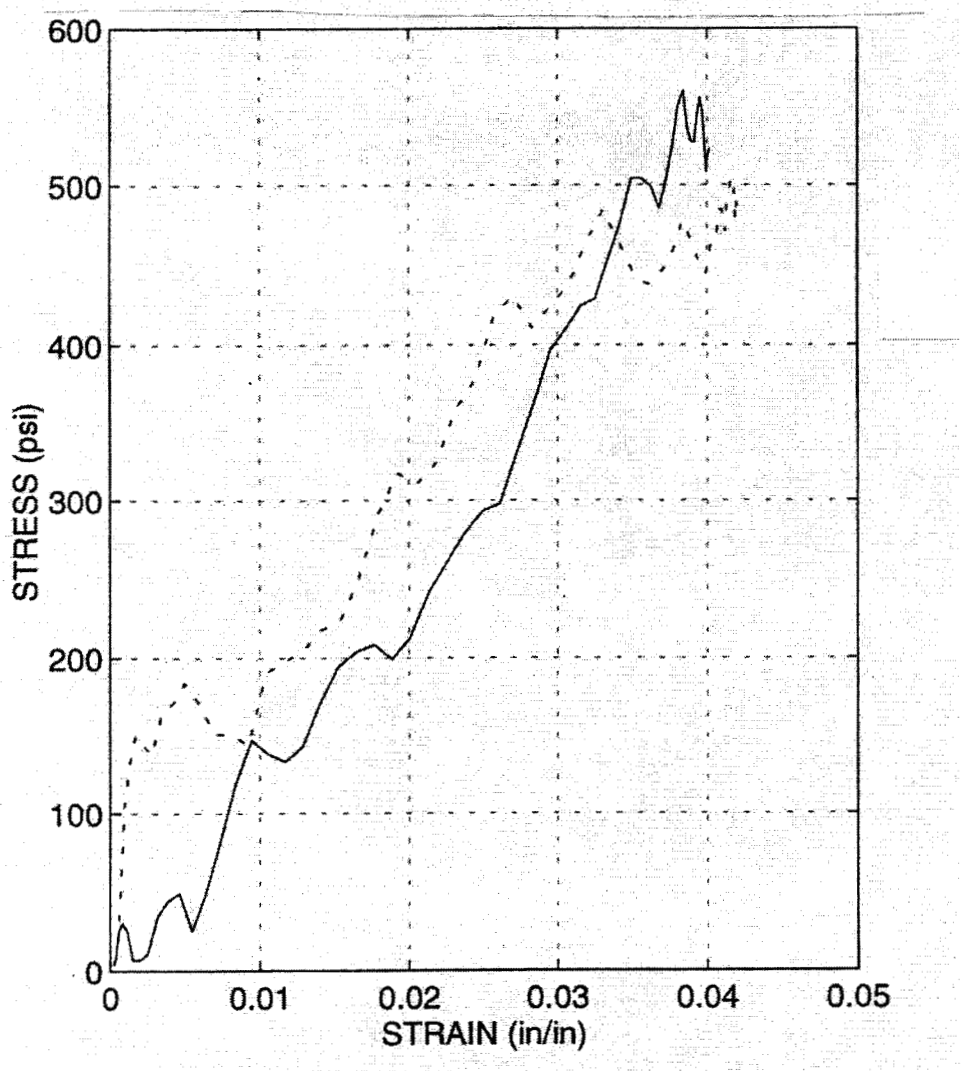

Figure 5: Constrained PMDI Foam with 10 pcf Density and 640 sec^{-1} Strain Rate
Solid – 40 fps Peak Velocity and 0.75 in. Length
Dashed – 80 fps Peak Velocity and 1.50 in. Length

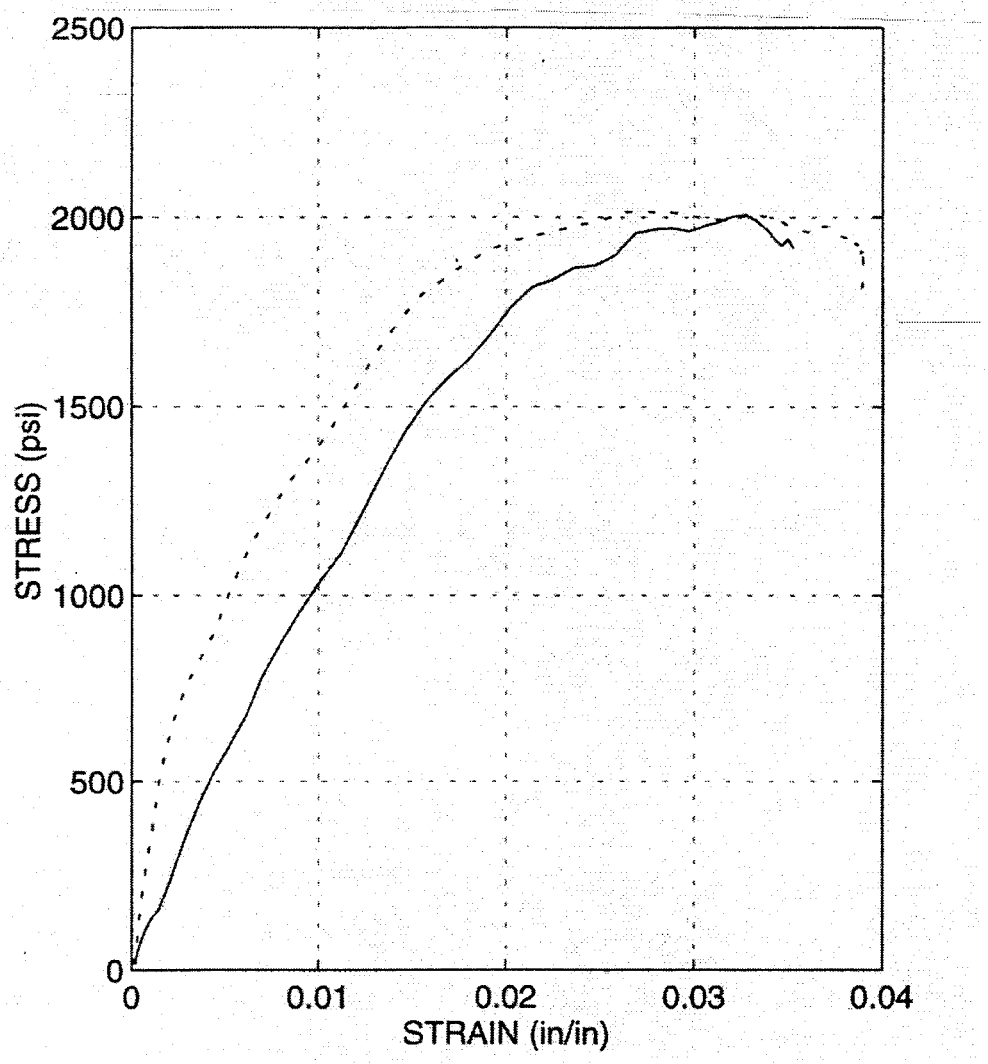

Figure 6: Constrained PMDI Foam with 20 pcf Density and 640 sec^{-1} Strain Rate
Solid – 40 fps Peak Velocity and 0.75 in. Length
Dashed – 80 fps Peak Velocity and 1.50 in. Length

The split Hopkinson bar testing of the foams continued with sample lengths that are similar to those found in the actual B61 assembly. The test matrix for these samples is shown in Table IV.

Table IV: Test Parameters for High Strain Rate Testing of 10 pcf and 20 pcf in Constrained and Unconstrained Geometries.

Length	Velocity	Strain Rate
0.15 in.	40 and 80 fps	3200 and 6400 sec^{-1}
0.35 in.	40 and 80 fps	1371 and 2742 sec^{-1}

The results from these tests are also shown as stress-strain plots in Figures 7-10 for the unconstrained samples and Figures 11-14 for the constrained samples. The displacements were approximately the same for both sample lengths in all cases and results in a lower strain for the longer sample (0.35 in.). This is a different results than that obtained for the longer samples of 0.75 in. and 1.50 in. nominal lengths. These samples did show different displacement or deformation for the two different lengths. The displacement or deformation for the 1.50 in. was approximately twice that for the 0.75 in.

As shown in Figures 7-10, there does not seem to be significant differences in the stress-strain response for the two sample lengths of the unconstrained foam and the test parameters as shown in Table IV. The general shape of the unconstrained foam plot is the same as before: a sharp linear increase in stress at low strains and a constant stress at higher strains. The peak stress values are summarized in Table V where it is evident that the 20 pcf foam is at least three times stronger than the 10 pcf foam in the unconstrained geometry.

Although the samples do deform during the passage of the stress wave through the sample, high-speed photometric measurements of the unconstrained 0.15 and 0.35 in. lengths indicate that these changes are not significant as discussed below. Consequently, the stress-strain plots may be considered true stress-true strain plots for the 0.15 and 0.35 in. lengths.

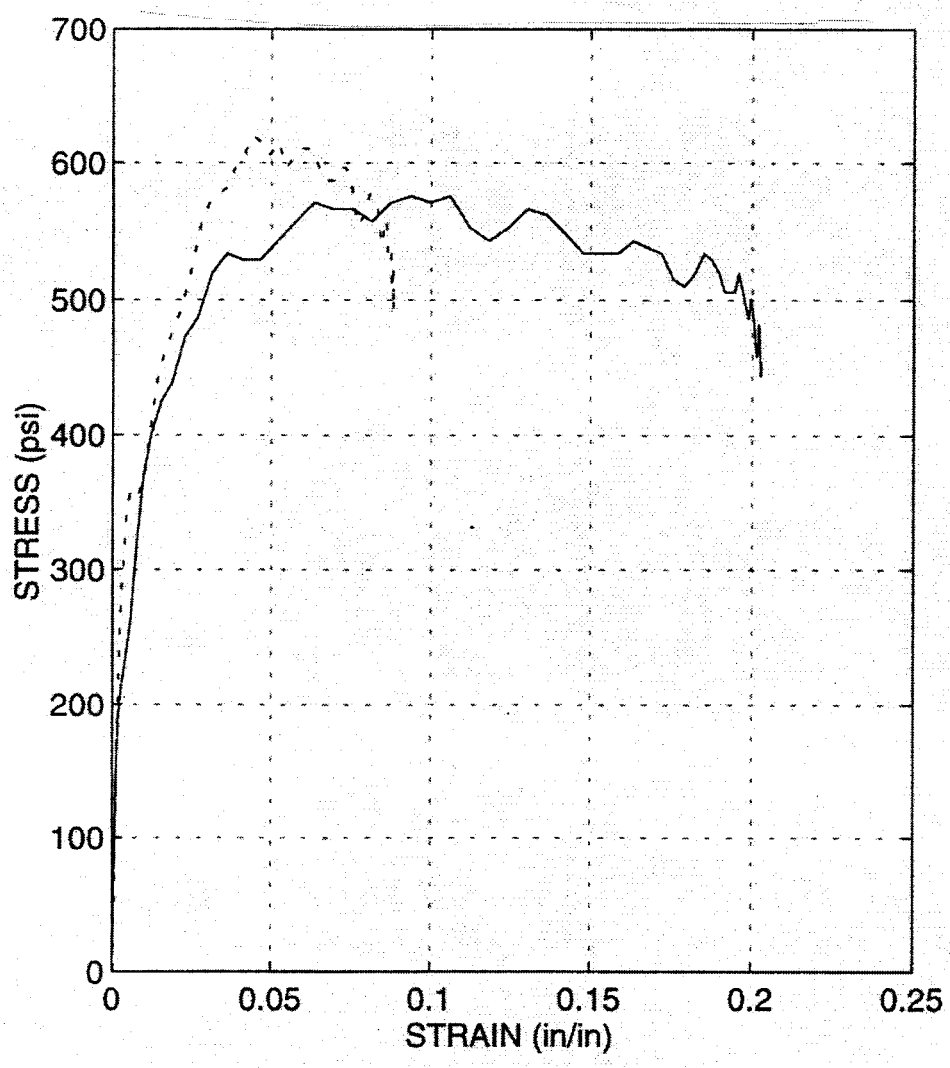

Figure 7: Unconstrained PMDI Foam with 10 pcf Density and 40 fps Peak Velocity
Solid – 0.15 in. Length
Dashed – 0.35 in. Length

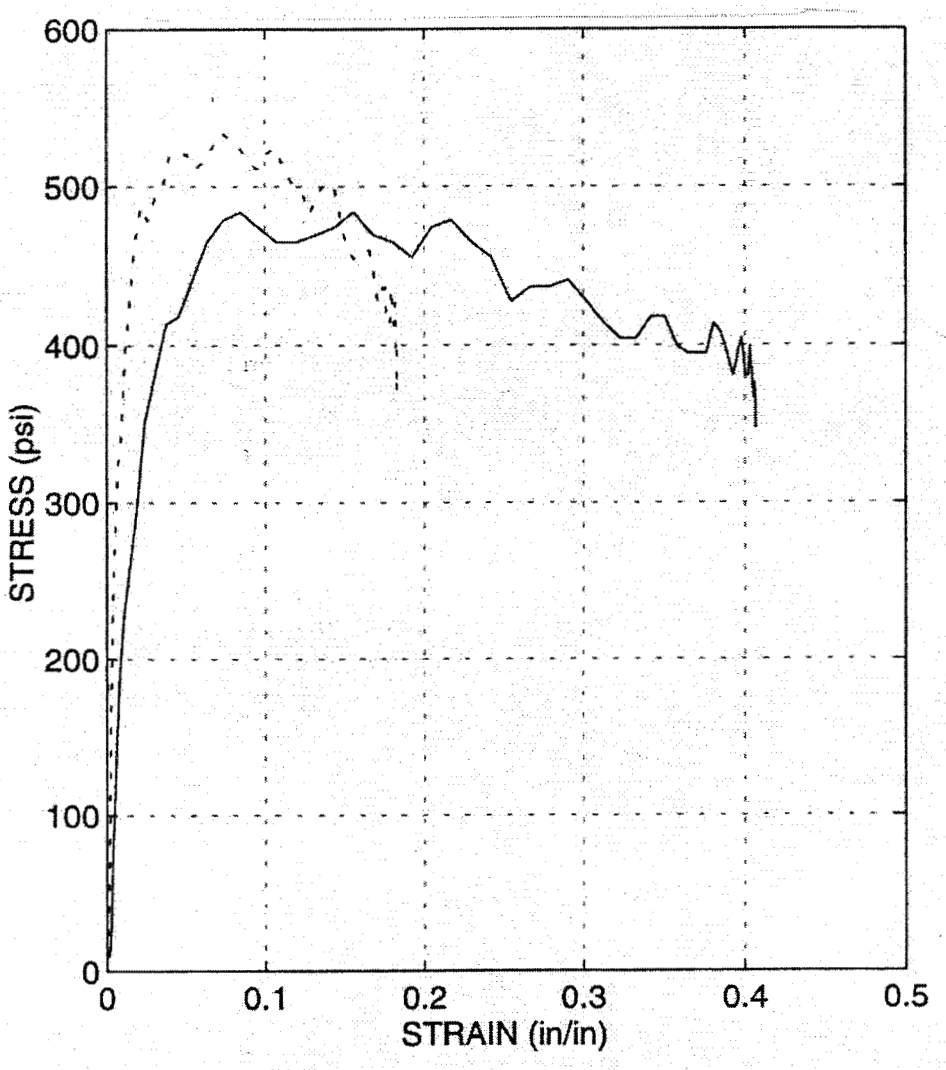

Figure 8: Unconstrained PMDI Foam with 10 pcf Density and 80 fps Peak Velocity
Solid – 0.15 in. Length
Dashed – 0.35 in. Length

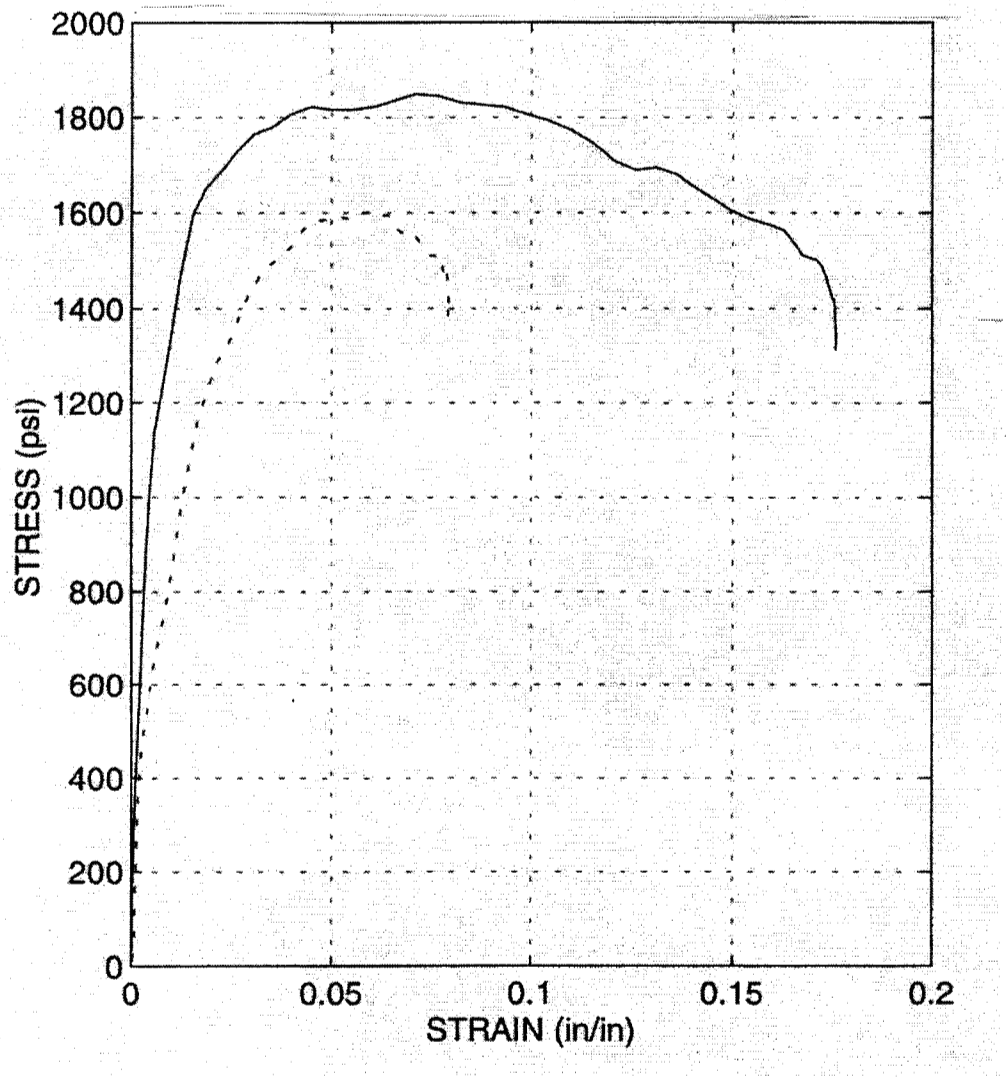

Figure 9: Unconstrained PMDI Foam with 20 pcf Density and 40 fps Peak Velocity
Solid – 0.15 in. Length
Dashed – 0.35 in. Length

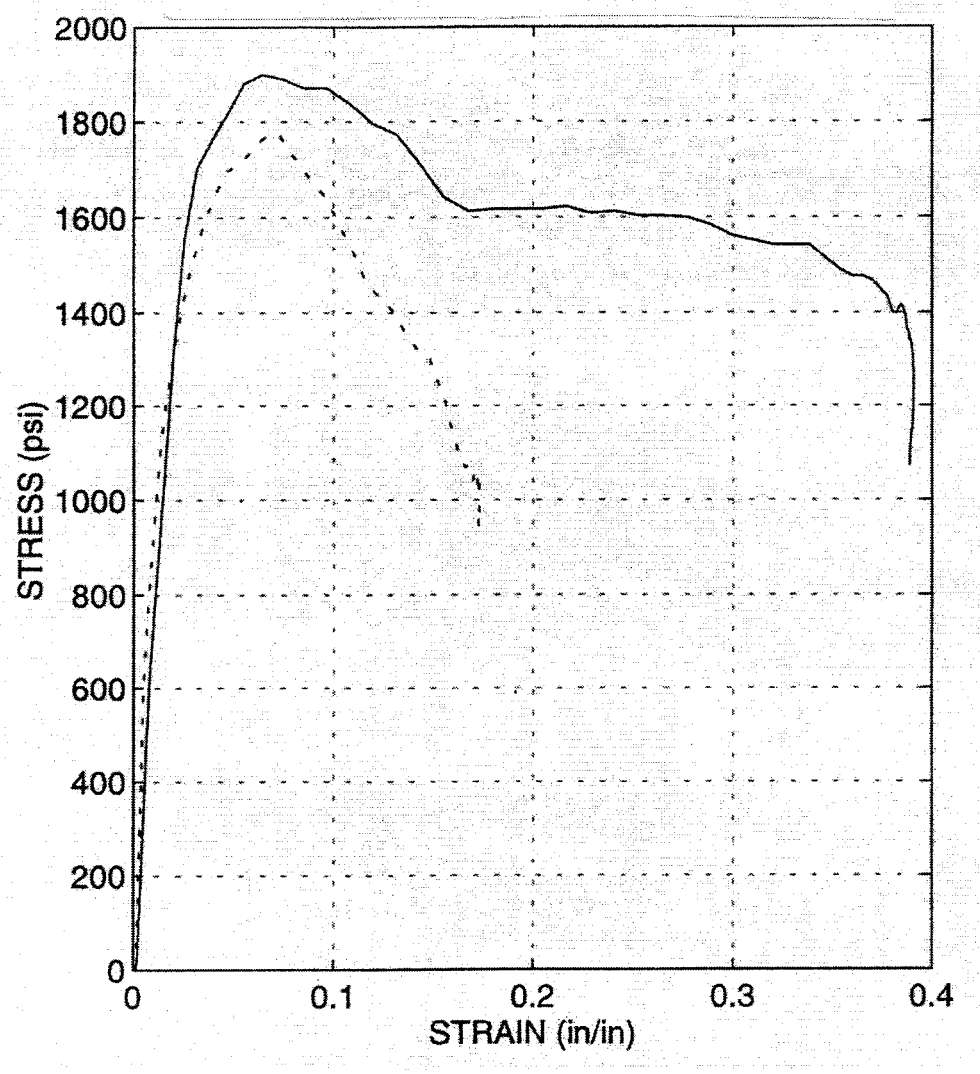

Figure 10: Unconstrained PMDI Foam with 20 pcf Density and 80 fps Peak Velocity
Solid – 0.15 in. Length
Dashed – 0.35 in. Length

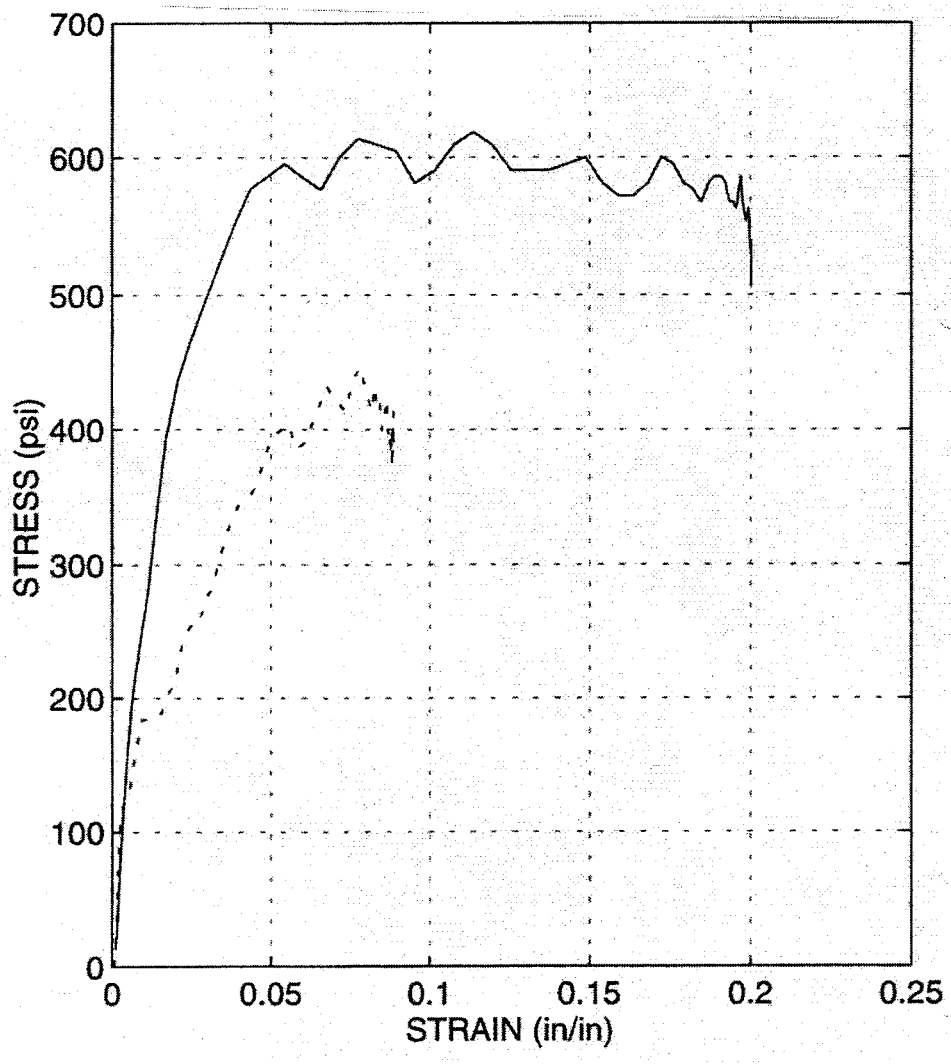

Figure 11: Constrained PMDI Foam with 10 pcf Density and 40 fps Peak Velocity
Solid – 0.15 in. Length
Dashed – 0.35 in. Length

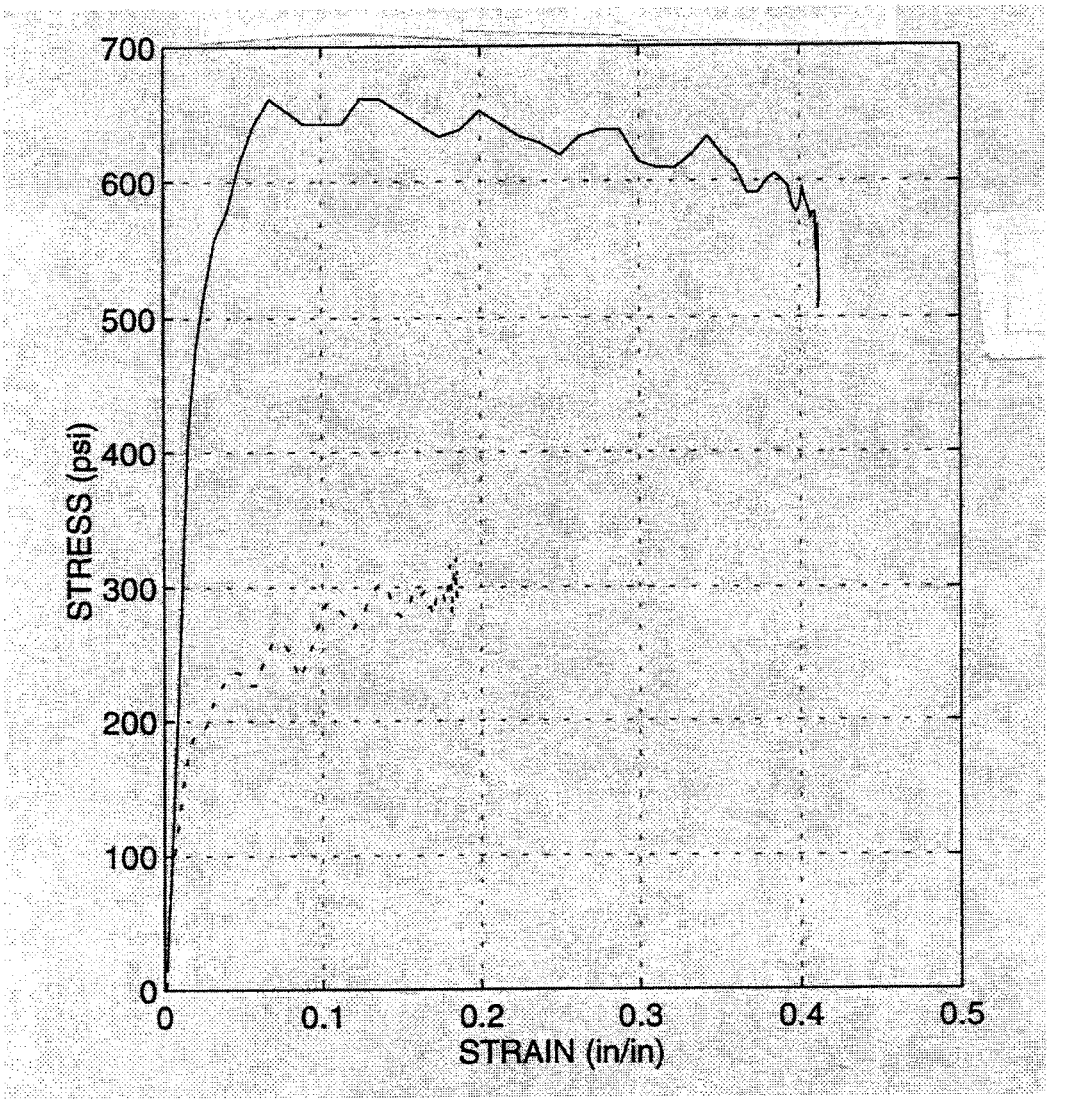

Figure 12: Constrained PMDI Foam with 10 pcf Density and 80 fps Peak Velocity
Solid – 0.15 in. Length
Dashed – 0.35 in. Length

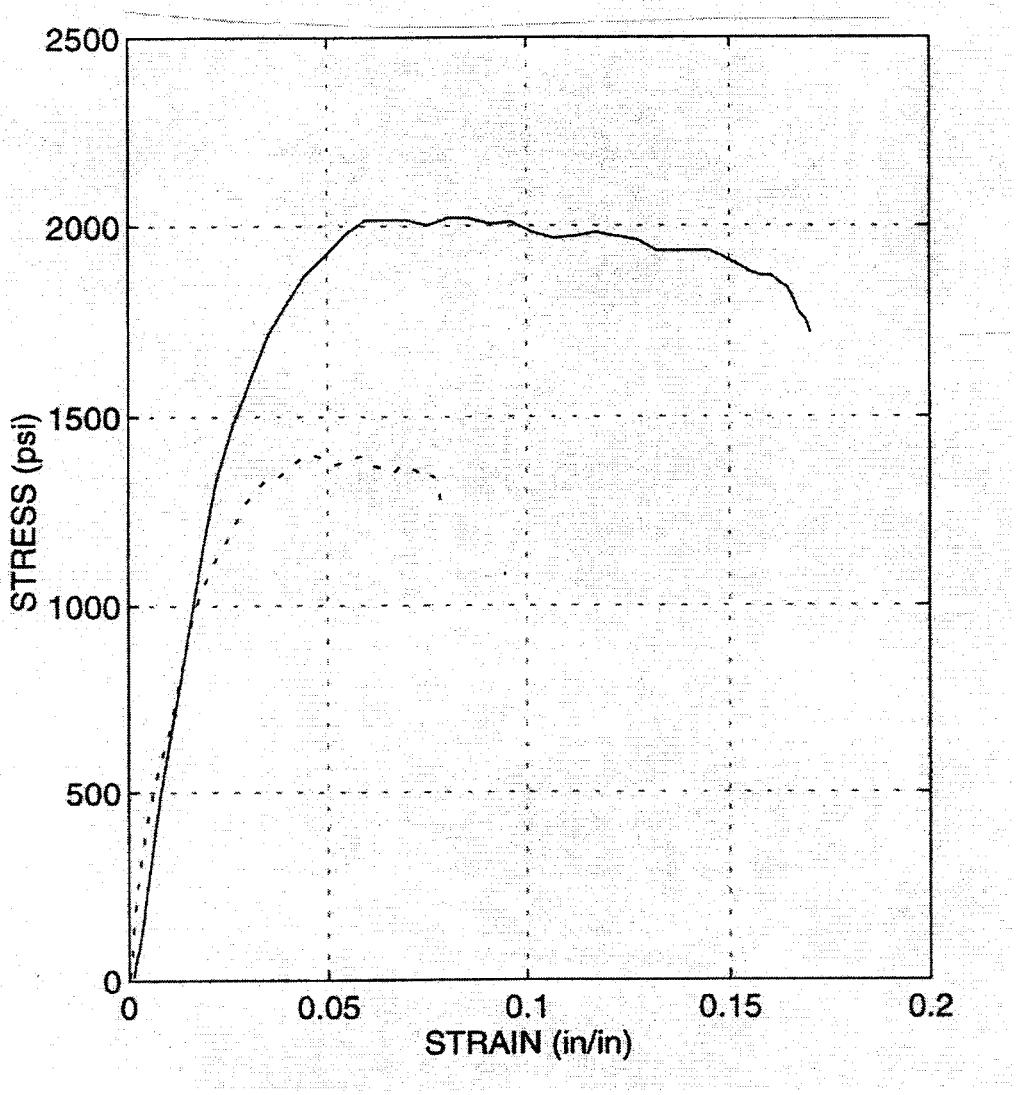

Figure 13: Constrained PMDI Foam with 20 pcf Density and 40 fps Peak Velocity
Solid – 0.15 in. Length
Dashed – 0.35 in. Length

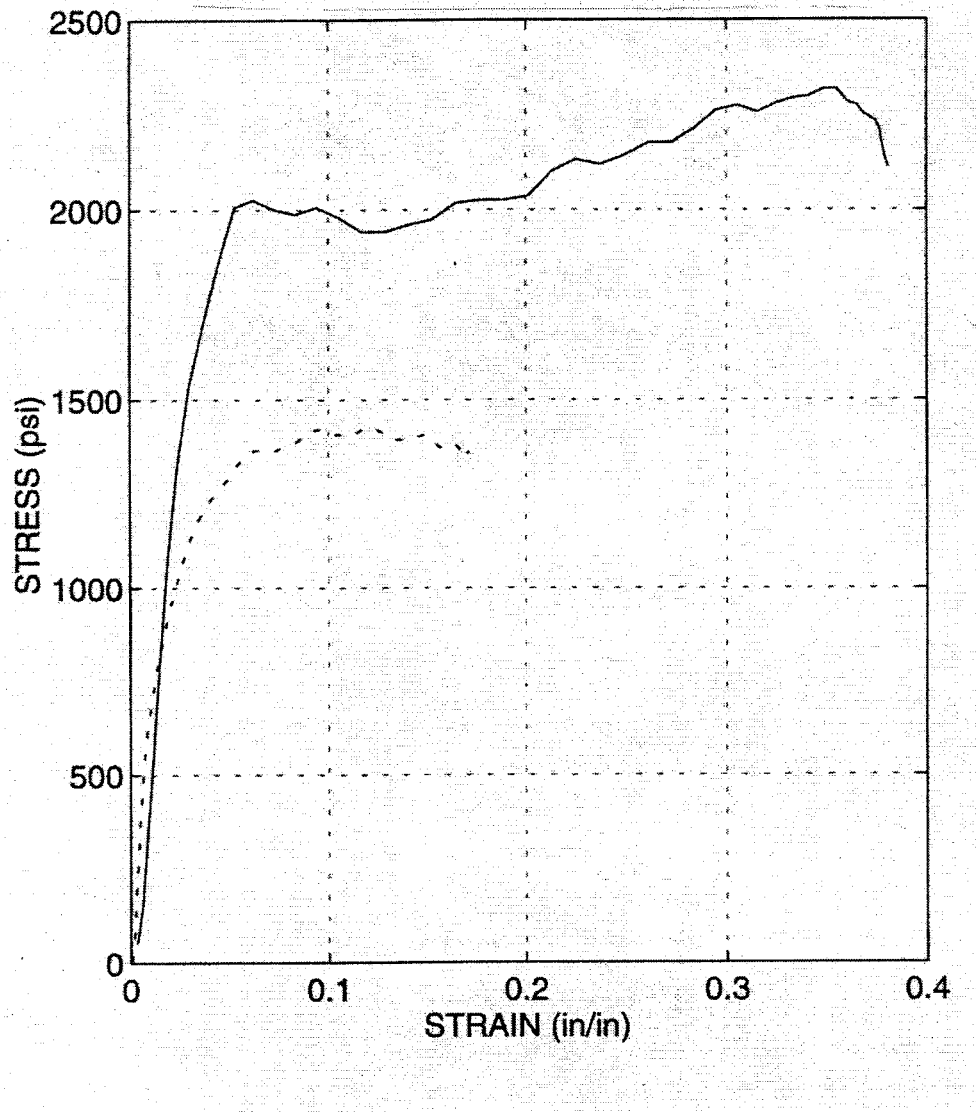

Figure 14: Constrained PMDI Foam with 20 pcf Density and 80 fps Peak Velocity
Solid – 0.15 in. Length
Dashed – 0.35 in. Length

Table V: Summary of Peak Stress Values for Split Hopkinson Bar Tests of Unconstrained Samples at 40 and 80 fps.

Velocity	10 pcf Density		20 pcf Density	
(Strain Rate)	0.15 in.	0.35 in.	0.15 in.	0.35 in.
40 fps (3200 and 1371 sec^{-1})	575 psi	600 psi	1850 psi	1600 psi
80 fps (6400 and 2742 sec^{-1})	475 psi	525 psi	1900 psi	1750 psi

The results for the constrained samples shown in Figures 11-14 **do** show significant differences for the two sample lengths. The thinner sample (0.15 in.) is stronger than the longer length sample (0.35) by 50% for the 10 pcf and 33% for the 20 pcf. The higher strength of the 0.15 in. sample may be due to pneumatic effects. That is, the air cannot escape as easily from the 0.35 in. samples, so the compressed air contributes to the cell rupture and significantly degrades the foam strength. The stress-strain curve for the contrained foam has the same general shape as the unconstrained foam at these strain rates instead of the approximately linear shape seen at the lower 640 $sec.^{-1}$ strain rate. The peak stress values for the constrained samples are shown in Table VI which shows that the 20 pcf foam is much stronger than the 10 pcf foam.

Table VI: Summary of Peak Stress Values for Split Hopkinson Bar Tests of Constrained Samples at 40 and 80 fps.

Velocity	10 pcf Density		20 pcf Density	
(Strain Rate)	0.15 in.	0.35 in.	0.15 in.	0.35 in.
40 fps (3200 and 1371 sec^{-1})	600 psi	425 psi	2000 psi	1400 psi
80 fps (6400 and 2742 sec^{-1})	650 psi	300 psi	2300 psi	1400 psi

High speed photometric measurements were made of the unconstrained foam (0.15 and 0.35 in. lengths) at the velocity of 40 fps to determine if the diameter changed significantly during the passage of the compressive stress wave through the sample and to confirm the displacements calculated from strain gage data. The average change in diameter was about 0.020 in. for both sample lengths ($\approx$ 5% change in area), and the displacements were approximately the same as those obtained by integrating the reflected strain wave. A video tape has been made from this high speed photography.

Optical Microstructure Analysis

Samples were cut parallel and perpendicular to the cylindrical axis, as shown in Figure 15, in order to quantify the "as-received" microstructure. Mounting, polishing, and imaging was identical to all other samples.

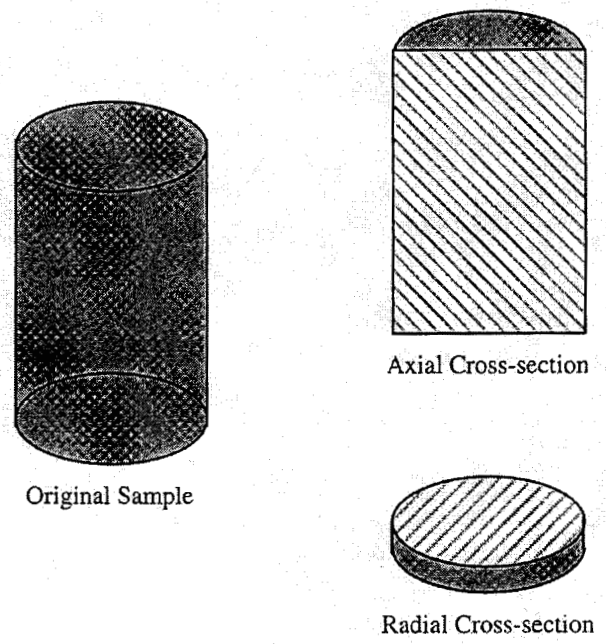

Figure 15: Schematic Representation of PMDI Foam Samples Show Both Axial and Radial Cross-Sections Taken From the Original Sample.

Figures 16a and 16b illustrate the microstructure of the radially unconfined 10 pcf foam in both the radial and axial directions, respectively. Elongation of large cells within the cross-section, as shown by arrows A in Figure 16a, are probably a typical imperfection because smaller cells within the cross-section did not appear to be distorted. Furthermore, the fact that the unconfined samples were

machined from a larger block suggests that possible edge effects could have been machined away leaving only homogeneous material. Examination of the sample in the axial direction, Figure 16b, did not reveal any further microstructural anisotropy, however the physical size of the sample (in the axial direction) precludes any statistical evaluation.

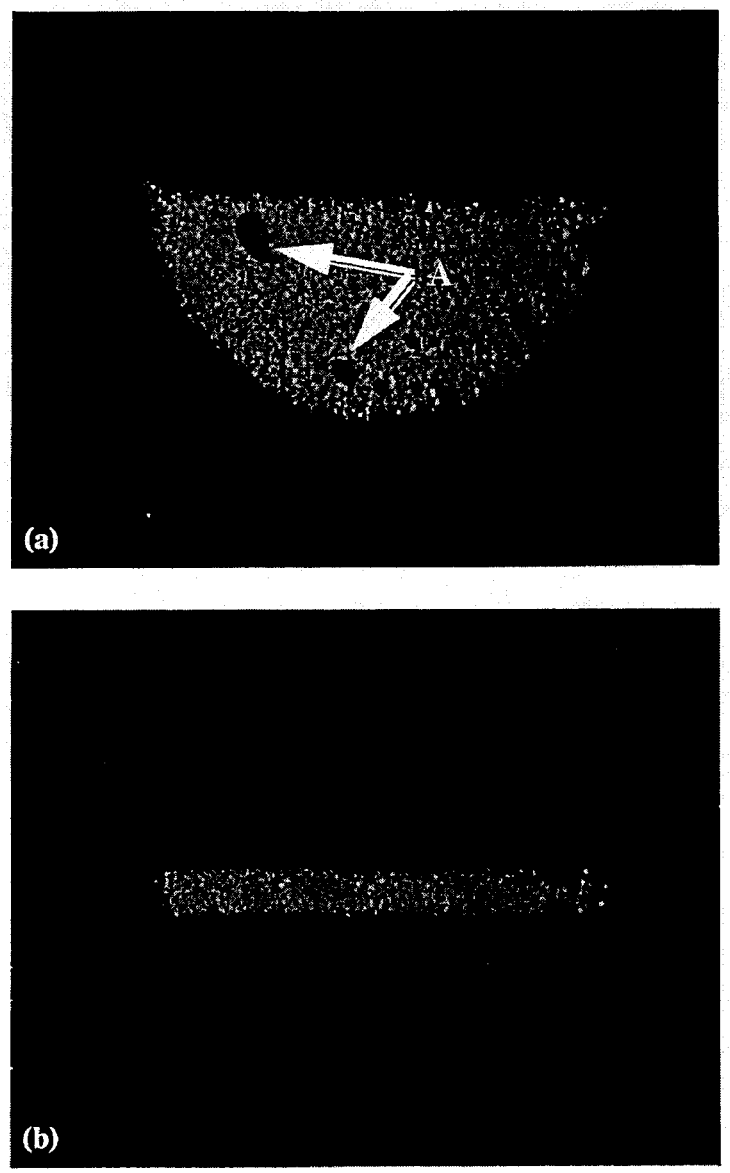

Figure 16: As-Received, 10 pcf PMDI Foam; (a) Radial Cross-Section Shows Large Cell Elongation (Arrows A), and (b) Axial Cross-Section.

Figures 17a and 17b illustrate the radially unconfined 20 pcf foam in both the radial and axial directions, respectively. No cell distortion was evident across either the radial or axial cross-sections as shown in Figures 17a and 17b,

respectively. Once again, the fact that the unconfined samples were machined from larger blocks suggests that possible edge anisotropy effects may have been eliminated in these samples.

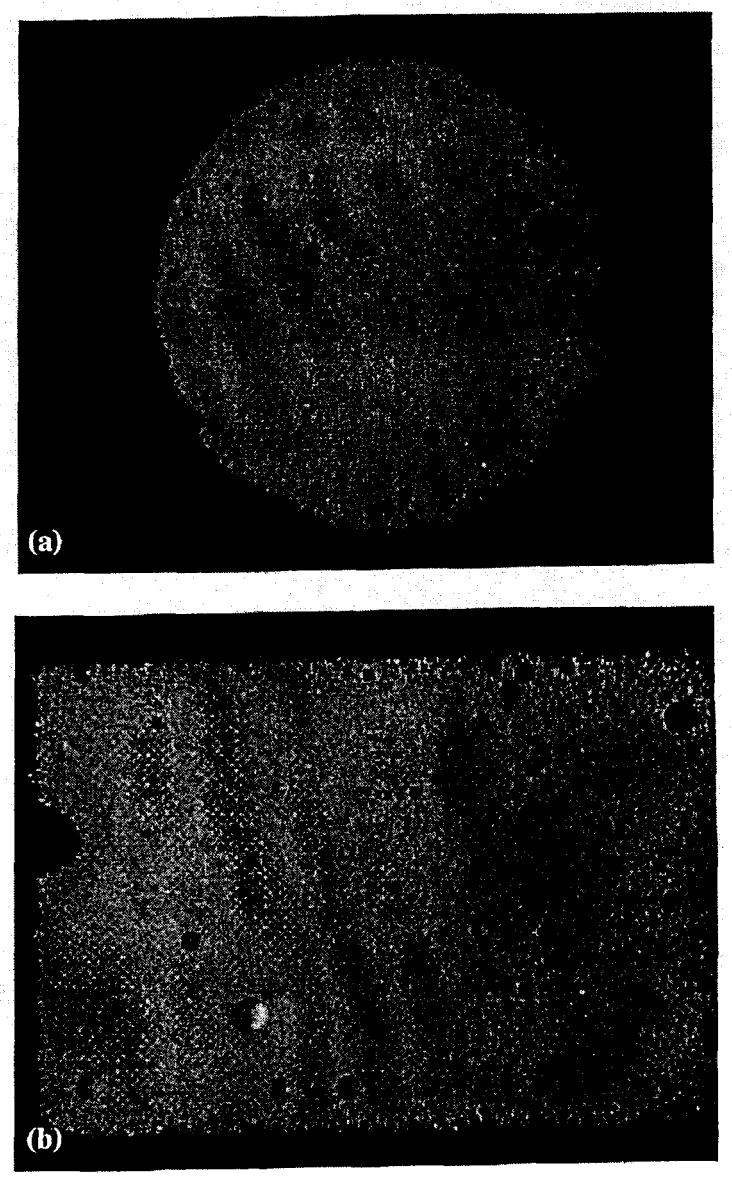

Figure 17: As-Received, 20 pcf PMDI Foam; (a) Radial Cross-Section and (b) Axial Cross-Section General Microstructure.

Microstructure of the as-received radially-confined 10 pcf foam is shown in Figure 18. The dark areas in the micrographs correspond to ruptured cells and the light areas correspond to regions of unruptured foam. It is evident from

Figure 18a that severe cell rupture, parallel to the steel cylinder wall, occurred during curing of the 10 pcf foam. It is also evident through close examination of the axial cross-section, Figure 18b, that exothermic cooling (i.e. preferential curing) occurred as evidenced by the graded structure in Figure 18b. It appears that an initial mechano-chemical bond formed with the steel tube wall and subsequently ruptured cells along the axial direction as the foam continued to rise and cure. Consequently, the radially-confined 10 pcf foam cells were ruptured during their curing within the steel tube.

Microstructure of the as-received radially-confined 20 pcf foam is shown in Figure 19. Distortion of individual cells, compressed in a direction perpendicular to the steel tube walls, shown in Figure 19a, suggests a cure texturing similar to the 10 pcf foam. The magnitude of distortion decreases as one traverses closer to the center. Given the higher strength of the 20 pcf foam, it is reasonable to assume that the individual cells were strong enough to resist rupturing during cure, thereby giving rise to the distorted geometry. Figure 19b shows elongation of individual cells close to the tube walls, suggesting a cure texturing similar to that of the weaker 10 pcf foam.

The impulse-loaded 10 pcf and 20 pcf rigid polyurethane foam samples were dry cut, encapsulated in epoxy, and pressurized to 310 kPa overnight. The hardened mounts were then cured for 8 hours at 32°C. A 600 grit finish was determined to be adequate for macro-photography. Images were recorded at magnifications ranging from 2.5x to 4.2x. The epoxy penetrated those areas of the foams where the cell walls had failed. The foams became translucent in those areas where the epoxy penetrated, thereby highlighting zones of damage.

Figure 20 illustrates the microstructures of the 10 pcf and 20 pcf, 1.5 in.-long, unconfined samples subjected to compressive impulse loading at an average strain rate of 640 $sec.^{-1}$. As noted on the micrographs, the compressive incident pulse was introduced from the left-hand side of the sample. Severe damage was clearly evident in the 10 pcf foam, Figure 20a, both on the left- and right-hand sides of the sample. No permanent deformation was observed in the center of the 1.5 in.-long sample; the cells in the central region appeared to retain their spherical geometry and none were ruptured. The greatest degree of damage was observed on the trailing side (right). It is not clear whether this damage was caused by the initial compression pulse or by subsequent loading. The fact that the major damage observed in the sample was closest to the sample/transmitted bar interface strongly suggests that a reflected tensile pulse caused the damage. Since the damage within the sample was not uniform, any representation of stress-strain data, at this sample length, is suspect.

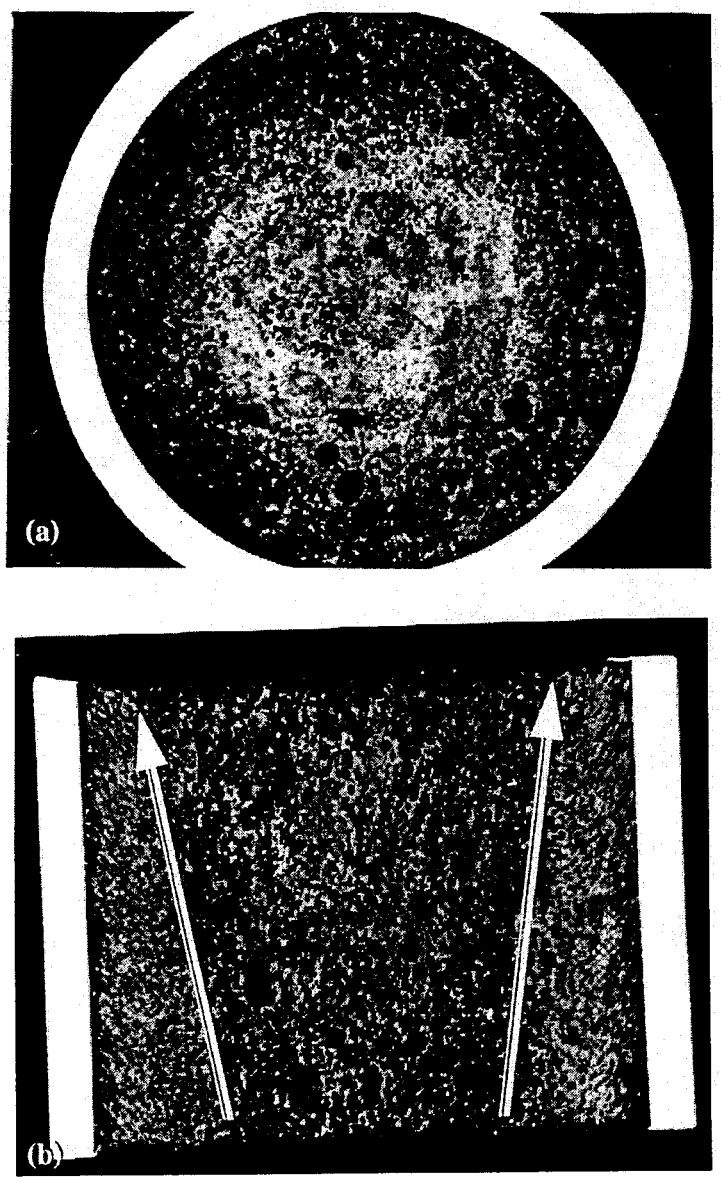

Figure 18: As-Received, Radially-Confined, 10 pcf PMDI Foam; (a) Radial Cross-Section, and (b) Axial Cross-Section Show Cell Rupture Along Steel Tube Walls and Damage Texturing (i.e. Preferential Curing) As Shown by Arrows.

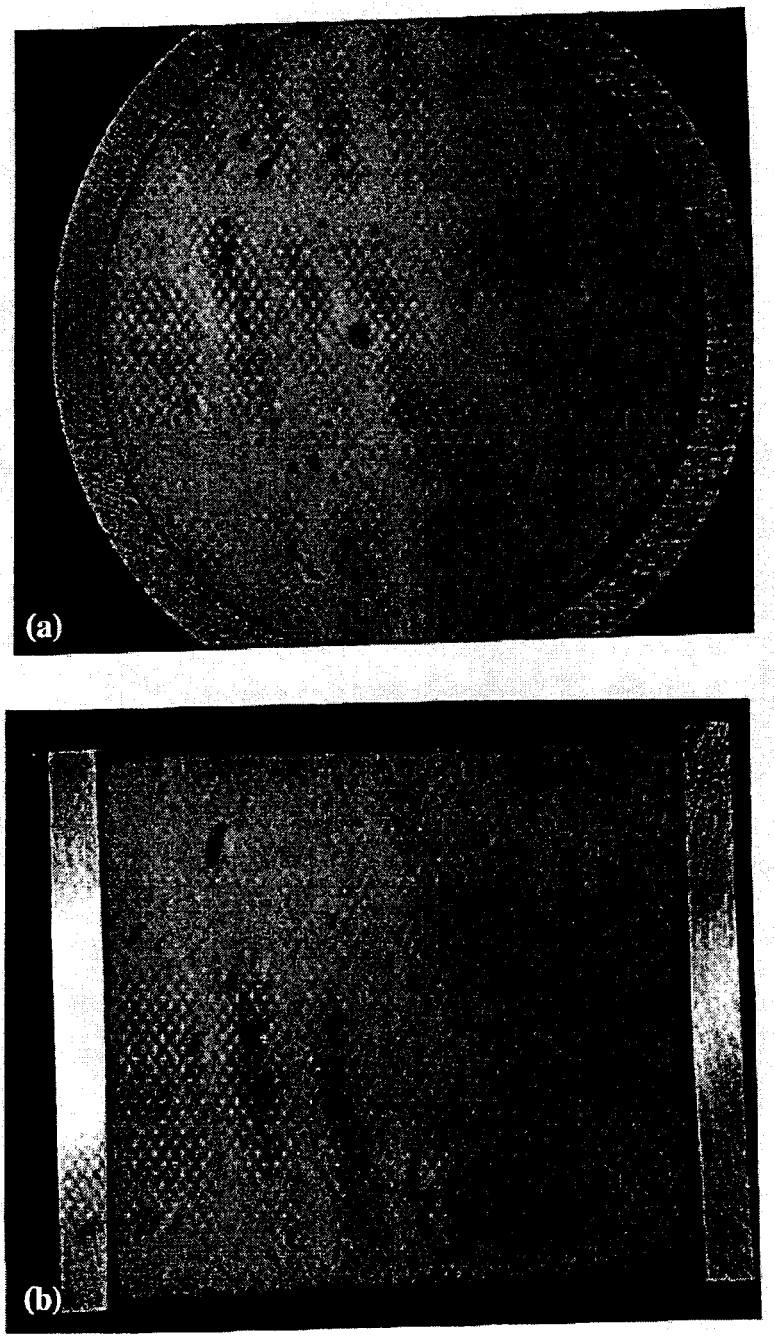

Figure 19: As-Received, Radially-Confined, 20 pcf PMDI Foam;
(a) Radial Cross-Section With Cell Compression
Perpendicular to the Steel Tube Walls, and
(b) Axial Cross-Section Cure Texturing Like 10 pcf Foam.

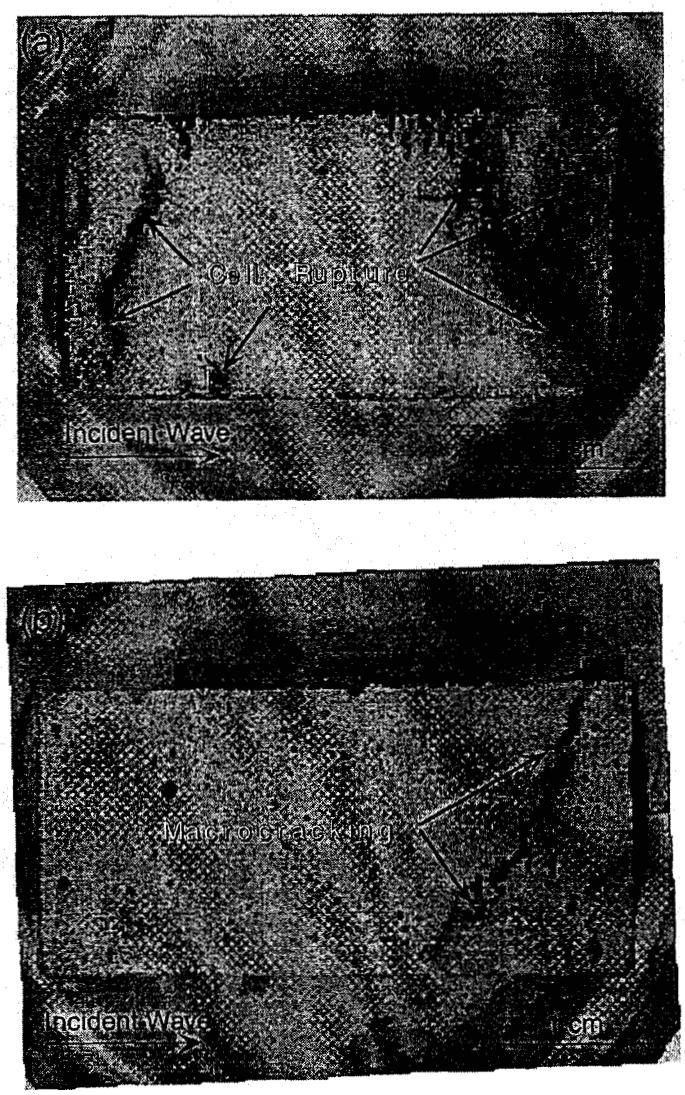

Figure 20: PMDI Unconfined Foam Samples, 1.5 in. Long, 640 sec. $^{-1}$ Strain Rate; (a) 10 pcf and (b) 20 pcf.

Microstructure of the 20 pcf foam, shown in Figure 20b, revealed similar features, but exhibited significantly less damage owing to an average increase in bulk strength with the increase in density. There appeared to be no compression-induced damage (cell shear or rupture) on the incident side; macrocracking, stemming from bulk cell rupture, was observed on the trailing-side. The increase in density from 10 pcf to 20 pcf served to increase cell wall thickness such that individual cells (and bulk structure) were able to withstand the initial compressive and subsequent reloading (tension/compression) to a greater degree than the lower density material. Indeed, the reported static strength increases more than 2x with an increase in density from 10 pcf to 20 pcf.

Figure 21 illustrates microstructures of the 10 pcf and 20 pcf, 1.5 in.-long, radially confined foam samples subjected to compressive impulse loading at an average strain rate of 640 $sec.^{-1}$. In contrast to the unconfined samples of same length, the radially confined samples exhibited a far greater degree of damage. Microstructure of the 10 pcf foam is illustrated in Figure 21a. The sample underwent a large degree of permanent damage along the incident wave side as evidenced by the dark areas representing ruptured and partially collapsed cells. It is clear that damage initiated along the steel tube walls (arrows) as material sheared under the compressive loading. It appears that the 10 pcf foam along the confining tube walls formed a strong mechano-chemical bond with the steel, elevating the local strength above that of the bulk foam. Rupturing of the cells under shearing led to general cell collapse in the bulk of the sample as evidenced by the failure path shown in Figure 21a illustrated by the arrows.

Microstructure of the 20 pcf radially-confined foam is shown in Figure 21b. Damage in the form of cell collapse parallel to the incident pulse, along the incident side (left) is clear, while bulk shearing is evident along the trailing edge (shown by the arrows). It is clear that the radial confinement served to increase the average transient strain levels within the sample as the pulse traveled through the sample as evidenced by deformation of individual cells (oblong shape) close to the regions of bulk shearing (arrows).

Microstructures of the 10 pcf and 20 pcf, 0.75 in.-long, unconfined samples subjected to compressive impulse loading at average strain rates of 640 $sec.^{-1}$ are shown in Figure 22. Both the 10 pcf and 20 pcf foams appeared to have survived the high-rate loading with no evidence of permanent deformation (in the form of collapsed or deformed cells, or bulk shearing). The absence of permanent damage, especially along the trailing edge, is interesting because it suggests a geometrical strengthening effect, although the magnitude of the incident pulse introduced to the sample was smaller than the 1.5 in.-long samples experienced.

Microstructures of the 10 pcf and 20 pcf, 0.75 in.-long, radially confined samples subjected to compressive impulse loading at an average strain rate of 640 $sec.^{-1}$

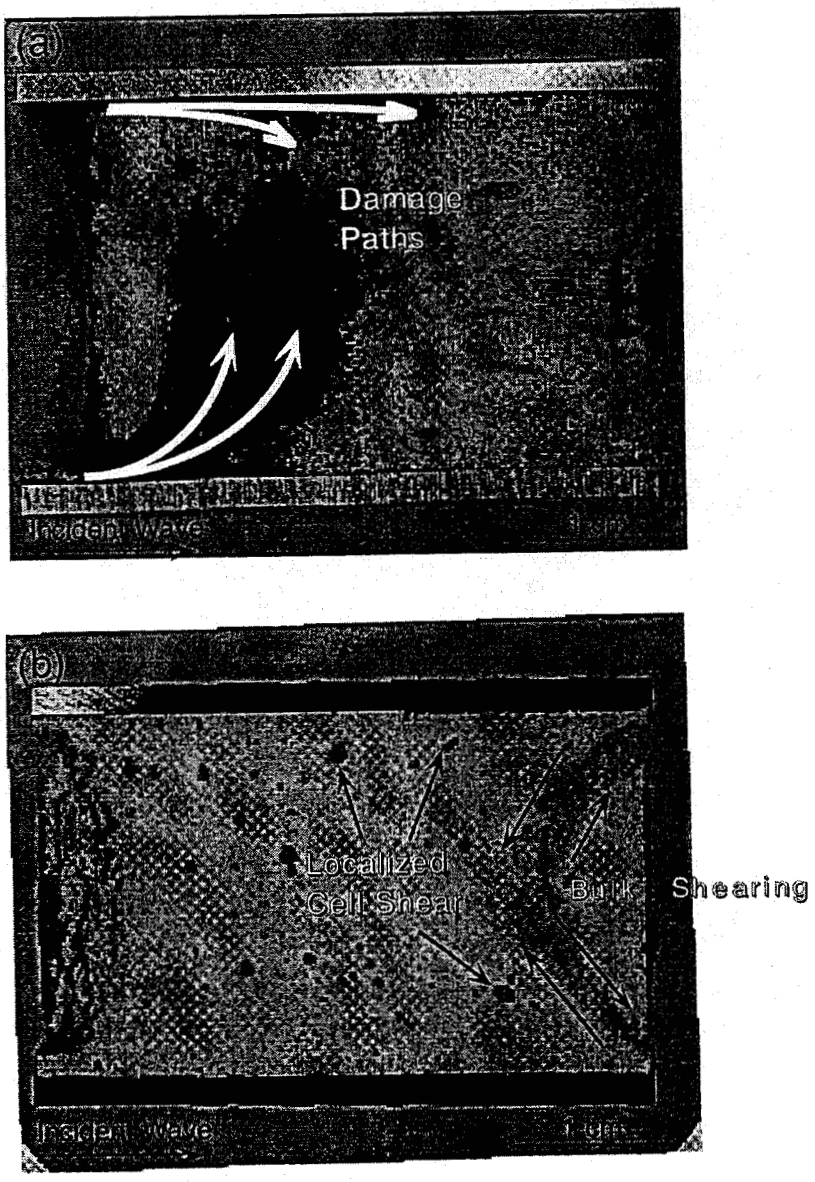

Figure 21: PMDI Confined Foam Samples, 1.5 in. Long, 640 sec.$^{-1}$ Strain Rate; (a) 10 pcf and (b) 20 pcf.

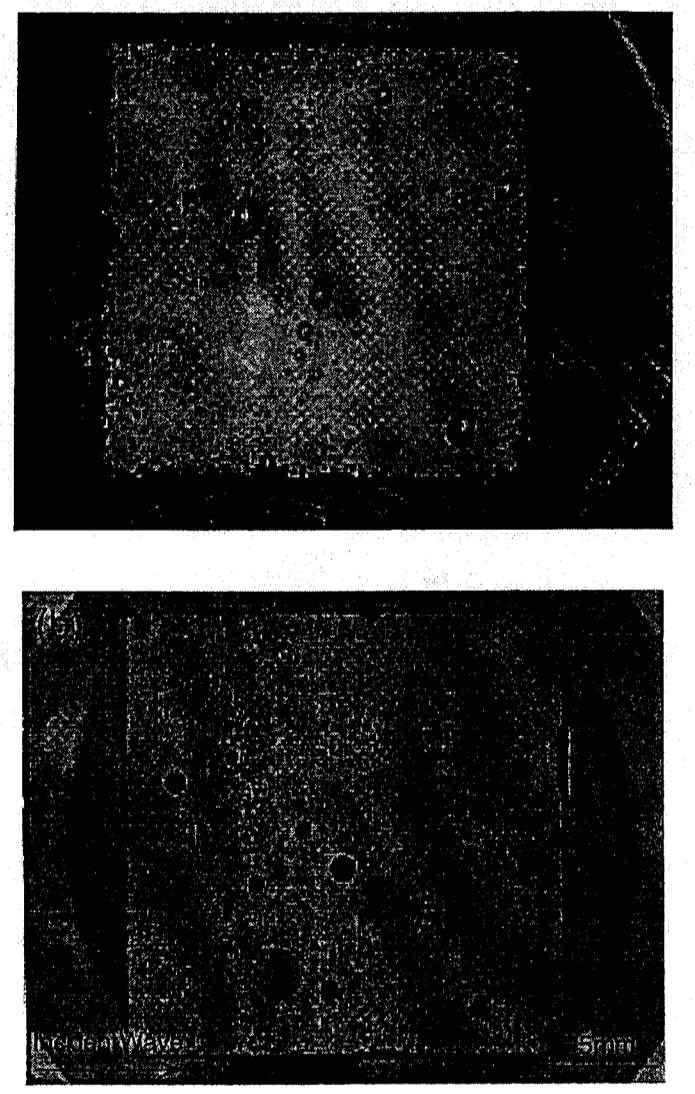

Figure 22: PMDI Unconfined Foam Samples, 0.75 in. Long, 640 sec.$^{-1}$ Strain Rate; (a) 10 pcf and (b) 20 pcf.

are shown in Figure 23. The 10 pcf foam revealed extensive damage throughout the cross-section, with total cell collapse at the incident wave interface. Severe shearing of the material, leading to total cell collapse along the tube walls extended from the incident interface to the trailing edge, as shown in Figure 23a. Damage within the sample primarily consisted of acute cell-wall rupture; the interior cells did not fully collapse.

The 20 pcf confined foam sample, shown in Figure 23b, did not reveal any bulk shearing or cell-wall collapse, however, permanent straining of the foam was evident from the geometry of the internal cells (oblong) as shown by the arrows in Figure 23b.

The microstructures of the 10 pcf and 20 pcf, 0.35 in.-long, unconfined samples subjected to compressive impulse-loading at an average strain rate of 1370 $sec.^{-1}$ are shown in Figure 24. Damage in the 10 pcf foam was evident along the incident side as completely collapsed cells creating a damage path in to the bulk of the sample as shown by the arrows in Figure 24a. Other damage within the sample consisted of partially compressed, but not ruptured, cells. The 20 pcf foam (1370 $sec.^{-1}$), shown in Figure 24b, revealed cell rupture within the interior of the foam initiated from the largest cells in the material, as shown by the arrows. Overpressure of the large cells seemed to collapse smaller adjacent cells, leading to the macrocrack formation shown in Figure 24b. Other cells within the sample were not damaged.

The 10 pcf foam impulse-loaded at an average strain rate of 2740 $sec.^{-1}$ experienced complete and total cell rupture and subsequent collapse. No un-ruptured cells were visible within this sample, so it is not shown. A 20 pcf sample at this same strain rate was not available, but the damage levels should be higher than the 20 pcf sample at 1370 $sec.^{-1}$ that had partial cell rupture and collapse.

The deformed microstructures of the 0.35 in.-long, radially confined samples subjected to compressive impulse-loading at average strain rates of 1370 $sec.^{-1}$ and 2740 $sec.^{-1}$ are shown in Figures 25 and 26, respectively. The 10 pcf confined sample in Figure 25a, revealed severe damage in the form of partially ruptured and completely collapsed cell walls throughout the entire length of the sample. The 20 pcf foam in Figure 25b, revealed some cell wall collapse parallel to the impact surface, however the bulk of the sample revealed no permanent damage.

At the average strain rate, 2740 $sec.^{-1}$, both the 10 pcf and 20 pcf foams showed significant damage. Figure 26a shows the 10 pcf foam structure following impulse-loading. Bulk shearing of the sample along the steel tube walls was evident leading to the total collapse of the cells in the interior of the sample. The 20 pcf foam in Figure 26b, also revealed significant damage within the interior of

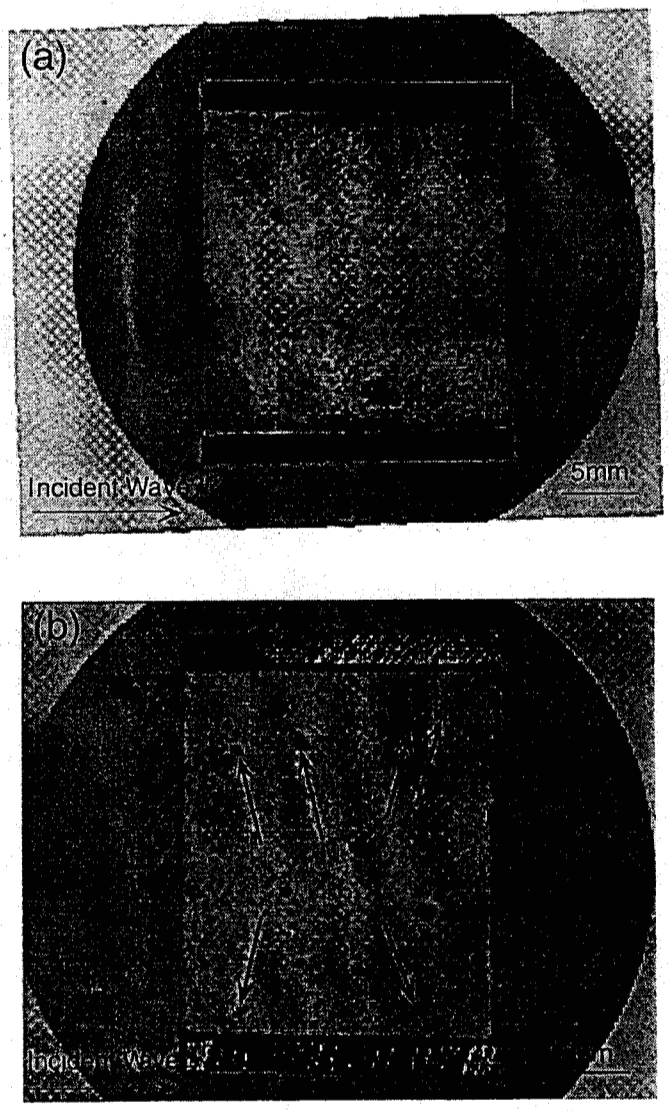

Figure 23: PMDI Confined Foam Samples, 0.75 in. Long, 640 sec.$^{-1}$ Strain Rate; (a) 10 pcf and (b) 20 pcf.

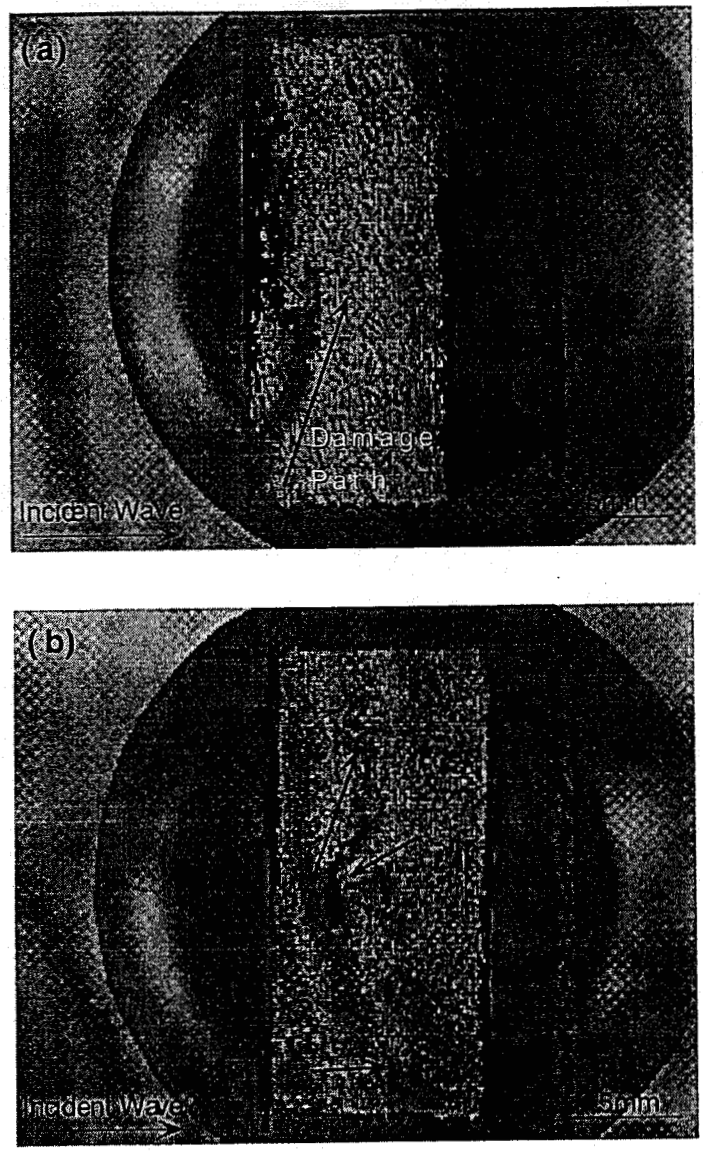

Figure 24: PMDI Unconfined Foam Samples, 0.35 in. Long, 1370 sec.$^{-1}$ Strain Rate; (a) 10 pcf and (b) 20 pcf.

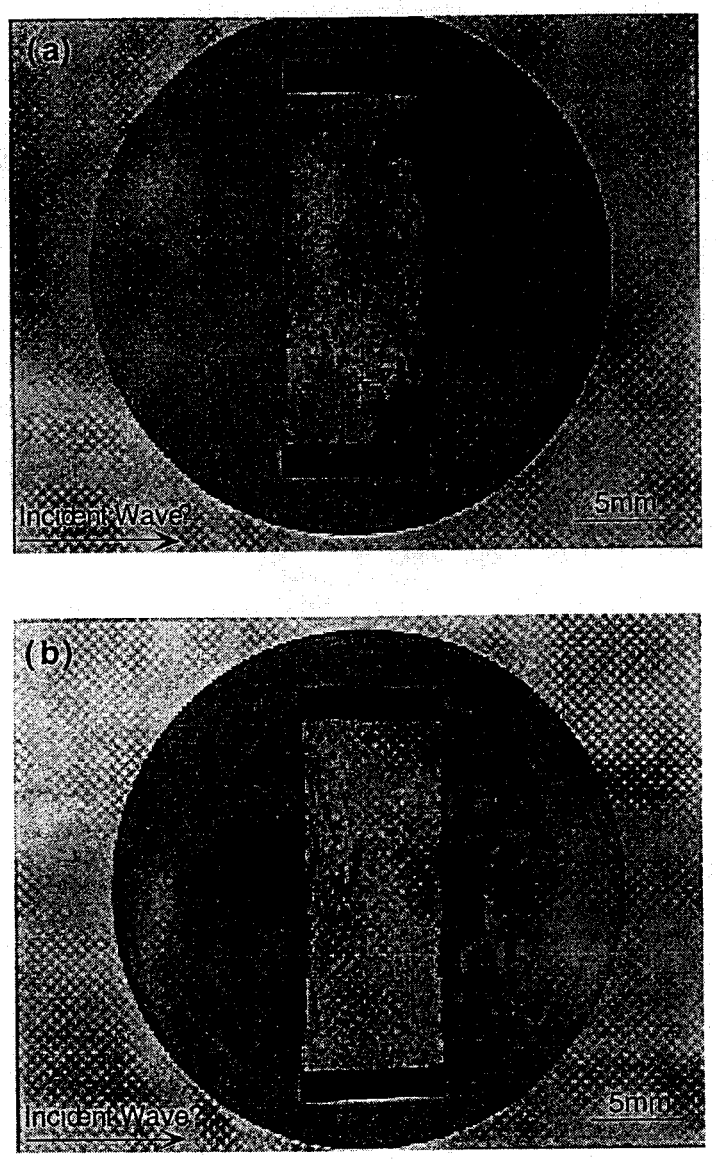

Figure 25: PMDI Confined Foam Samples, 0.35 in. Long, 1370 sec.$^{-1}$ Strain Rate; (a) 10 pcf and (b) 20 pcf.

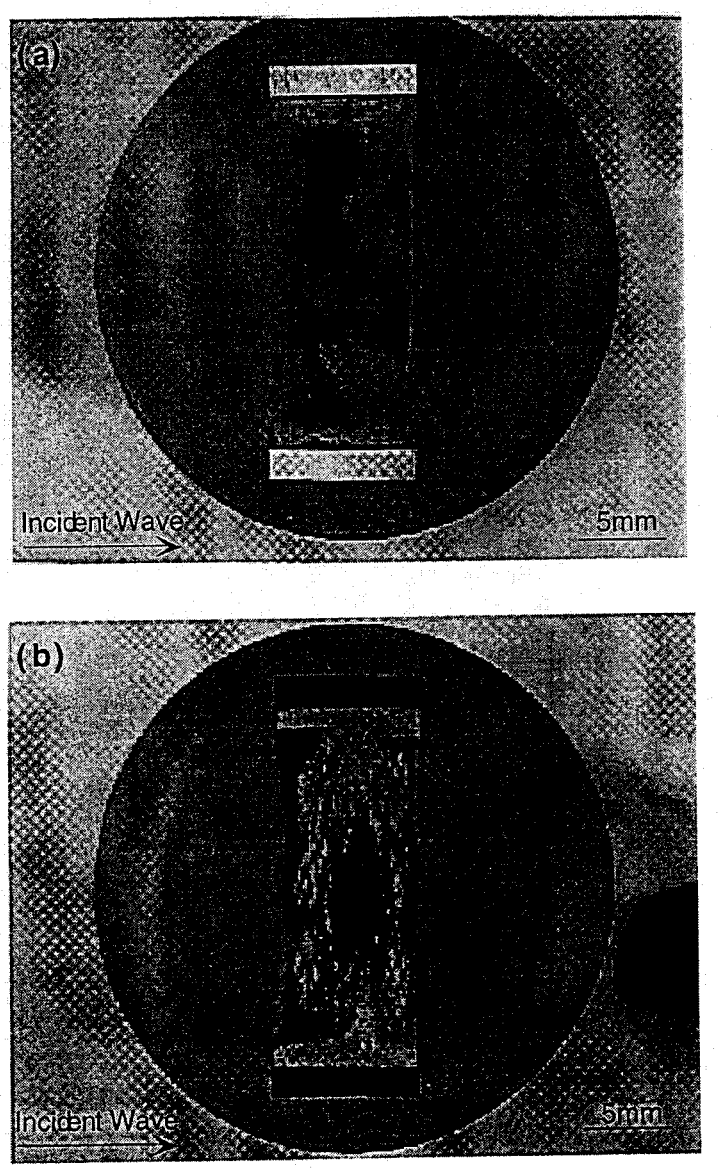

Figure 26: PMDI Foam Samples, 0.35 in. Long, 2740 sec.$^{-1}$ Strain Rate; (a) 10 pcf and (b) 20 pcf.

the sample on both the incident and trailing sides. No shearing of the sample along the steel tube walls was evident in this sample, suggesting that the strength of the 20 pcf foam exceeded the strength of the mechano-chemical bond along the wall.

Microstructure of the 0.15 in.-long, 10 pcf and 20 pcf samples at 3200 sec.$^{-1}$ and 6400 sec.$^{-1}$, confined and unconfined, exhibited bulk shearing with complete sample translation following impulse load with one exception. Consequently, there was almost total rupture and collapse of the interior cells. Overpressure of the 0.15 in.-long unconfined samples indicates that the shorter lengths do not have time to radially expand during compression. The overpressure causes immediate rupture and collapse before elastic radial expansion can occur indicates a strong geometrical contribution to failure at these impulse levels and average strain rates. The exception to these results is the confined 20 pcf foam at the 3200 sec.$^{-1}$ strain rate. This sample had partial cell rupture, however no bulk shearing was observed. Since there was total catastrophic failure of most of the 0.15 in. long samples, these micrographs are not shown in this report.

Uncertainty Analysis

The uncertainty in these measurements and results are attributed to two sources: the uncertainty in the sample dimensional measurements and the uncertainty in the strain gage calibrations. The uncertainty the sample dimensional measurements is assigned as $\pm$ 2.0%. The strain gage and data acquisition uncertainty is monitored on a continual basis in the SNL Mechanical Shock Laboratory as required by the SNL Specification 9958003 [4]. These requirements include the performance of both the hardware (strain gages, amplifiers, digitizers etc.) [4,5] and the software IMPAX that controls the data acquisition system through a computer [4, 6, 7]. The current data acquisition system and software meet these requirements within $\pm$0.5%, and documentation of these results is maintained in the Mechanical Shock Laboratory. A study of the uncertainty in strain gage measurements has shown this uncertainty to be + 6.0 % [8]. Consequently, the two uncertainties in these data are the uncertainty in the sample dimensional measurements, $\pm$ 2.0 % and the uncertainty in the strain gage calibrations of + 6.5 %, 95% confidence level [8]. These two uncertainties are considered random, so they may be combined in an uncertainty analysis with a 95 % confidence level as [9,10]:

$$w_T = \sqrt{w_s^2 + w_{sg}^2} \qquad (1)$$

where: w_T = total uncertainty,
w_s = sample dimensional measurements uncertainty , $\pm$ 2.0 %, and
w_{sg} = strain gage calibrations uncertainty, + 6.5 %.

The value of the total uncertainty, w_T, is $\pm$ 6.3 % and is typical for the measurements made in the SNL Mechanical Shock Laboratory.

Conclusions

A split Hopkinson bar capability has been demonstrated, and stress-strain plots have been derived for PMDI foam. The stress-strain plots are true stress-strain plots for the sample lengths of 0.15 in. and 0.35 in. The fundamental principles governing use of a split Hopkinson pressure bar are: (a) the incident, transmitted, and striker bars remain elastic, (b) wave propagation within the pressure bars is one-dimensional , and (c) the sample undergoes uniform deformation. Although (a) and (b) were satisfied in this endeavor, uniform deformation did not appear for the larger sample lengths, 1.5 and 0.75 in. That is, the stress-strain characteristics should not be used to derive constitutive data for the larger sample lengths, 1.5 and 0.75 in. Non-uniform damage was observed in the unconfined 1.5 in.-long PMDI foam samples subject to compressive impulse loading. Suppression of radial expansion in 1.5 in.-long samples increased the relative levels of damage with respect to radially unconfined samples. Strong mechano-chemical bonds formed along the steel tube walls in the radially confined samples, causing non-uniform deformation across the sample cross-section; the method of pouring foam into a steel tube for radial confinement is not recommended for further use. Damage occurred by overpressuring of individual cells, creating an avalanche effect leading to subsequent overpressuring of adjacent cells, rupture, eventual collapse, and permanent strain accumulation. Finally, the level of damage in the PMDI foams increased with increases in strain rate (i.e. increases in input energy), and decreases in sample thickness.

Recommendations for Future Work

It is recommended that the testing be continued with ambient testing of the TDI foam for comparison with the PMDI foam characteristics. Further, a more realistic constrained foam geometry should be tested for both PMDI and TDI foams. The constrained foam was constructed by pouring the foam into tubes and allowing the foam to bond to the inside of the tube during the curing process. A more realistic geometry would be to put the foam into the tubes to simulate a B61 configuration. Therefore, it is recommended that radial confinement be investigated through the use of slip-collars that fit over both the sample and the split Hopkinson pressure bars. Close tolerance slip collars allow comparison of identical material (with respect to the unconfined samples) and allow axial compression to occur. This approach will eliminate the pre-ruptured cells in the radially-confined samples, cured within the steel tubes that may alter mechanical material properties. Additionally, rigid foams (or brittle materials in

general), are not homogeneous, and demand that statistical testing and analysis be employed to properly analyze test data. Finally, the testing of both foams should be conducted at both hot and cold temperatures.

Acknowledgements

The authors would like to thank Pete B. Rand, Dept. 1811, for his initial consultations and advice about the test configuration and matrices. The authors would also like to thank Pete B. Rand, Consultant, and Michael K. Neilsen and William M. Scherzinger, Dept. 9123, for their careful review of this report. The financial support by Walter J. Errickson, Dept. 2111, and Aaron Hillhouse, Dept. 2112, is also gratefully acknowledged.

References

1. Lindholm, U. S., "Some Experiments with the Split Hopkinson Pressure Bar," *Journal of the Mechanics and Physics of Solids*, Vol. 12, pp. 317-335, 1964.
2. Follansbee, P., "High Strain Rate Compression Testing," *Metals Handbook*, Vol. 8, 9th Edition, pp. 198-217, American Society for Metals, Metals Park, 1985.
3. Neilsen, M. K., H. S. Morgan, and R. D. Krieg, "A Phenomenological Constitutive Model for Low Density Polyurethane Foams, "," SAND86-2927UC-71, National Technical Information Service, 5285 Port Royal Road, Springfield, VA 22162, April 1987.
4. Ulibarri, Davie, and Kuehnle, "Mechanical Shock Test Instrumentation," Sandia National Laboratories Specification 9958003-4, 1992, pp. 1-19.
5. Bateman, V. I., "Data Acquisition System Hardware Fidelity Check Procedures," February 14, 1997, pp. 1-21.
6. Bateman, V. I., "Software Management Plan for Software Supporting Production Lot Acceptance Testing," January 11, 1996, pp. 1-5.
7. Bateman, V. I., "Software Quality Requirements for Area I Mechanical Shock Laboratory," Issue A, January 11, 1996, pp. 1-10.
8. V. I. Bateman, W. B. Leisher, F. A. Brown, and N. T. Davie, "Calibration of a Hopkinson Bar With a Transfer Standard," *Shock and Vibration Journal*, Vol. 1, No. 2, pp. 145-152 (1993).
9. Doebelin, E. O., "Measurement Systems Application and Design," *McGraw Hill Book Company*, New York, N. Y., 1983, pp.57-60.
10. Abernathy, R. B. "Measurement Uncertainty Handbook," *Instrument Society of America*, Research Triangle Park, N.C., 1980.

Distribution:

1	MS0329	G. E. Sleefe (2614)
1	MS0329	D. A. Hoke (2614)
1	MS0447	E. J. Connors (2111)
1	MS0447	W. J. Errickson (2111)
1	MS0483	A. L. Hillhouse (2112)
2	MS0553	V. I. Bateman (9126)
1	MS0553	F. A. Brown (9126)
1	MS0555	M. S. Garrett (9122)
1	MS0557	T. J. Baca (9125)
1	MS0824	J. L. Moya (9130)
1	MS0847	H. S. Morgan (9120)
1	MS0847	R. A. May (9126)
1	MS0847	W. M. Scherzinger (9123)
1	MS0847	M. K. Neilsen (9123)
1	MS0847	D. R. Martinez (9124)
1	MS0888	P. B. Rand (1811)
1	MS9018	Central Technical Files Dept. 8945-1
2	MS0899	Technical Library (9616)
1	MS0612	Review & Approval Desk Dept. 9612 For DOE/OSTI